Chapter

The Busemann Air Intake for Hypersonic Speeds

Sannu Mölder

Abstract

A review and summary is presented of hypersonic air intake technology highlighting design objectives, basic flows, airframe integration, flowpath modification and intake flow startability. Taylor-Maccoll equations and Busemann flow are presented as the basis for constructing modular Busemann intakes. Wavecatching (streamline tracing), morphing and foreshortening are presented to show that (a) wavecatching is a useful technique to create modular startable intakes; (b) morphing is useful in integrating the intake shape with other geometric requirements of the airframe and combustor; and (c) foreshortening leads to minor gains in intake performance but large weight savings. A novel, *strong shock* method is presented, which uses strong-shock boundary conditions for designing spontaneously startable, modular Busemann intakes of high performance. This allows pre-determination of Busemann intake startability; offering great simplicity in the search for flowpath surface shapes that yield startable intakes with high compression, high efficiency and supersonic exit flows. Busemann flow contains unique fluid mechanical features: (a) a flow passage from a uniform, high Mach number flow, to another uniform, lower Mach number flow; (b) internal, convergent flow with an inflected surface; (c) conical flow where high gradients are near the center line and milder gradients are at the walls; (d) an axisymmetric and conically symmetric centered compression fan; (e) a free-standing conical shock, bounding irrotational flow. These are unique and fortuitous virtues, being significant in making the Busemann streamtube and its flow characteristics a suitable basis for designing high performance air intakes for hypersonic airbreathing engines.

Keywords: hypersonic air intake, Busemann design performance

1. Introduction to hypersonic air intake technology

There is a need for transporting man, machines, materials and munitions through Earth's atmosphere at high speed. Engines that propel fast airplanes are either rockets, or engines of airbreathing type. Turbojets, ramjets and scramjets (supersonic combustion ramjets) are types of airbreathing engines for propelling airplanes in the sensible atmosphere. The practical airbreathing engine for hypersonic speeds (above 5000 km/h) is the scramjet. A schematic is shown in **Figure 1**. The key components of the scramjet engine are the intake, the combustor and the nozzle. Mission studies have shown that a scramjet-propelled vehicle can provide a 2-hour travel time to most places on Earth or it can aid in the task of boosting vehicles to Earth orbit.

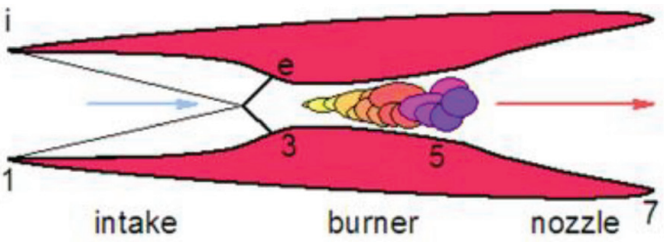

Figure 1.
The scramjet and its three components.

The air intake is one of the three essential components of supersonic and hypersonic airbreathing engines. It conditions the approaching freestream airflow for the combustor and the nozzle, compressing the airflow for best performance of the downstream components. For best overall engine performance, it must do so with minimal losses. The intake's performance can be thought of in terms of what the intake does and how well it is doing it-the *capability* and the *efficiency*. Capability can be quantified by such variables as the ratio of entry-to-exit Mach number, ratio of flow areas (contraction) or ratio of pressures (compression). Efficiency can be measured by the total pressure recovery or the entropy rise from entry to exit. These considerations of "what" and "how well" are governed by the First and Second Laws of Thermodynamics. Both capability and efficiency are highly dependent on the geometry of the intake surface. This raises additional design concerns about the intake's length and weight as well as exit flow inclination and uniformity, and the startability of the intake flow. These factors have a major effect on the intake's performance and on its design.

1.1 Intake design objectives

The hypersonic intake decelerates and compresses the freestream airflow as it flows into the combustion chamber. In doing this, (a) the intake flow must start and achieve the required decrease in Mach number with a high thermodynamic efficiency; (b) the compressed airflow, flowing into the combustor, should be uniform and stable; (c) the intake should operate efficiently and stably over the entire flight envelope bounded by flight Mach number, altitude and angle of attack; (d) the intake structure should be as light as possible; (e) drag of external surfaces and aerodynamic heating loads should be minimal; (f) for useful engine operation, the intake duct shape and flight conditions must be such that the intake airflow is predictable, properly conditioned (uniform in some sense) and aligned with the combustor walls as it flows into the combustor. These requirements for intake design are often contradictory, making it difficult to attain optimum individual operating conditions simultaneously. For example, in a fixed-geometry intake, flow starting and the need for substantial Mach number reduction pose a very serious geometric flowpath contraction contradiction that leads to an onerous design task.

Thermodynamic cycle calculations of high Mach number airbreathing engines, such as scramjets, have shown that the engines should have air intakes that contract and compress the flow by factors of 6–10 and 10–20 respectively and that this contraction and compression should be done with minimal loss of total pressure. Aside from high contraction and compression, the attainment of efficient intake performance is critically dependent on the freestream Mach number and the lateral and stream-wise contours of the intake surface, both being factors in determining the character of the flow in the intake and its performance.

Since all these design concerns are intake shape-dependent, it is most convenient and reasonable to start an iterative type intake design procedure with the selection

of an intake shape that is known to produce a geometrically simple, compressive flow. Flow on a plane inclined wedge, Prandtl-Meyer flow and flow over a circular cone, as well as their combinations, have been used extensively as starting points for supersonic intakes because their aerodynamic characteristics are simple and easily predictable analytically. These "textbook" flows are usually adaptable to physical variations in geometry where shape change may be required for optimised performance over a range of Mach numbers and to ensure intake flow startability. In selecting such simple and easily predictable flows and their streamlines, for intake applications, we search for geometric streamlines that join a uniform and parallel freestream entry flow to an equally uniform and parallel exit flow. For most intakes the exit flow direction should be the same as that of the freestream. The flow compression in the intake should be longitudinally distributed so as to be isentropic at the high Mach number, upstream end of the intake. Minimal shock losses are obtained when compression through shock waves occurs at the lower Mach number, downstream end. So as to minimize viscous losses, all surfaces should contribute usefully to the compression task by individually supporting positive pressure gradients. The desirable qualities should not deteriorate significantly at off-design conditions of flight Mach number, altitude or angle of attack.

1.2 Simple planar and axial flows

Scramjet engine thermodynamic cycle calculations and combustor performance place a requirement on the hypersonic air intake to reduce the freestream Mach number by a factor of about three and to do so with a total pressure recovery of at least 0.5. These design targets can be met by employing combinations of simple inviscid flows that are assembled to form the intake flowpath. The simple flows can be based on either planarly symmetric (planar) or axially symmetric (axial) supersonic "text-book" flows. In planar flows, flow properties are the same in parallel geometric planes. In axial flows, flow properties are invariant in planes around a common axis. Because of planar or axial symmetry, the number of independent spatial geometric variables, needed to specify the flow, is reduced from three to two—a great simplification for design and analysis. These simple flows also possess radial symmetry in that there is no variation of flow properties along flat planes (planar flow) or cones (conical Taylor-Maccoll flow). Use of simple flows with flat plate and conical symmetry allows the number of spatial variables that are required to specify and describe the flow, to be further reduced by one, so that only one independent geometric variable remains—a further simplification for intake design and analysis. Examples of such commonly used simple planar flows are the flow behind a flat oblique shock and Prandtl-Meyer flow. Commonly used simple axial flows are the flow over a cone and the Busemann flow. Simple flows and their combinations do not carry shocks that are curved in the flow plane; this keeps the intake flows irrotational and uniform. An important part of intake design consists of combining and connecting the simple flows to yield the desired intake performance. The other part consists of using selected streamline sheets of these flows to form desired flowpath shapes—a technique called *wavecatching*.

The focus in this paper is on the use of *axial*, internal flow elements (basic flows) [1–3], rather than planar flow elements, to construct intake flow paths. The axisymmetric intake attains most of its compression by flow convergence rather than flow turning or shock deflection. The converging flow is isentropic, it is similar to sink flow and it causes a Mach number decrease which leads directly to weak terminal shocks waves and efficient intakes with high capability. The internal converging flowfield is the most important feature of an axial flow intake.

Problems of viscous losses and flow starting are eased by use of wavecatcher technology, providing leading edge truncation and sweep and by the fact that high adverse pressure gradients occur in the inviscid core flow rather than in the wall surface boundary layers. Hypersonic intakes that utilize axisymmetric compressive basic flows with specified entrance and exit shapes have received attention because of their high performance (capability and efficiency) and analytical simplicity [4–24].

A preferred geometry for a scramjet combustor is a duct with a circular cross section because of its superior ability to withstand both heat and pressure loads. Frictional losses are also at a minimum for such a duct since a cylinder has the smallest surface area for a given cross-sectional area. This leads to a cylindrical (axially symmetric) geometry as being desirable also for the intake that is attached to the front of the combustor duct. The same circular exit geometry for the intake is demanded by a gas turbine engine, in this case because the axial compressor face is circular. Towards these ends, it is pertinent to study an axisymmetric flow and it is entirely fortuitous that axisymmetric, conical, Taylor-Maccoll flow provides a streamtube shape [1, 2] that satisfies the above intake design requirements, both geometric/structural as well as aerodynamic [3]. In recognition of Adolph Busemann's pioneering work [1] on such streamtube shapes, they are called Busemann flows and Busemann intakes. References [1–18, 24] all concern Busemann flow.

1.3 Intake flow processes and inward/outward flows

The reduction of Mach number, in the various basic flows, is accomplished by one or more fluid mechanical mechanism: (a) compressive flow *turning*; (b) flow *convergence* with area contraction and compression in a converging passage and (c) flow *deflection* through an oblique shock. Flow turning and contraction are isentropic processes leading to no loss in efficiency. Flow deflection through an oblique shock entails an entropy increase—a loss in intake efficiency. If shocks are needed to deflect or re-direct the flow then they should be as weak as possible, occurring at the lowest possible Mach number (e.g., Busemann shock). Planar flow turning by Prandtl-Meyer-type flow requires much turning to accomplish a significant Mach number reduction, so that, after P-M turning, strong shocks are required to re-direct the flow back to the freestream direction for the combustor. On the other hand, isentropic Mach number reduction by area contraction leads to a rapid streamwise Mach number reduction when the flow is axial. In such flows, Busemann flow being typical, there is comparatively little flow turning towards the center line, the compression being accomplished by area contraction and, as a result, there is no need for much deflection (re-turning) by a shock at the exit. Also, since there is considerable Mach number reduction in the converging flow, the terminal shock faces a reduced Mach number. This weaker terminal shock minimizes efficiency losses. The axial flow intakes derive their high efficiency from the axial convergence, being only little degraded by flow deflection through the terminal shock. The axial Busemann intakes have been mistakenly labeled as "inward turning" even when part of their converging flow is turning outward, away from the axis. We suggest dropping the "inward turning inlet" terminology in favor of "axial flow intake" or "converging flow intake," because their fundamental and characterizing distinction is axial convergence. It is precisely the lack of much "inward turning" that leads to the high performance of Busemann intakes. It would be better to use the flow-related and meaningful concepts of *turning, convergence and deflection* to characterize intake flow types in general. Isentropic turning, as in

P-M flow, may have to be used where variable geometry demands the use of planar flow. The resulting flow turning, away from the flight direction, has to be compensated by lossy oblique shock deflections. On the other hand, flow convergence, such as occurs in sink flow, is an effective mechanism because it is isentropic and involves no flow turning. Deflection occurs through an oblique shock; it is non-isentropic and it should be used only when there is no other possibility of orienting the flow. It should not be used to reduce the Mach number. A practical flow, such as Busemann [1], incorporates all three of these aerodynamic mechanisms as they interactively contribute to intake performance.

The three modes of compression are illustrated in the Prandtl-Meyer intake, the Oswatitch intake and the Busemann intake (**Figure 2**). The Prandtl-Meyer intake obtains performance by isentropic *turning* through the compression fan, followed by *deflection* through the oblique shock; there is no *convergence*. The Oswatitch intake has flow *divergence* and *turning* followed by *deflection* through a shock. The Busemann intake has *turning* and *convergence* followed by shock *deflection*. Three intake models were designed to reduce the Mach number from 8.33 to 4.8 with a static pressure ratio of 26.8. All three intakes were tested in a gun tunnel [11] at Mach 8.33 and it was found that, for the same amount of contraction, the inviscid total pressure recoveries of the Busemann, Oswatitch and Prandtl-Meyer intakes were 0.983, 0.763 and 0.763. Experimental total pressure recoveries were 0.484, 0.485 and 0.240. The reason for the differences stems from the fact that the surface area and consequently the viscous losses, were greatest for the Prandtl-Meyer intake. Sidewalls, needed to contain the planar Prandtl-Meyer flow, did not preserve the intake's efficiency but contributed to the surface area and viscous losses. The lack of an extensive leading edge and attendant viscous flow contributed to the efficiency of the Oswatitch intake. These results illustrate the superiority of axial over planar basic flows where it is the Mach number reduction, achieved by convergence, that leads to the high performance of the Busemann intake.

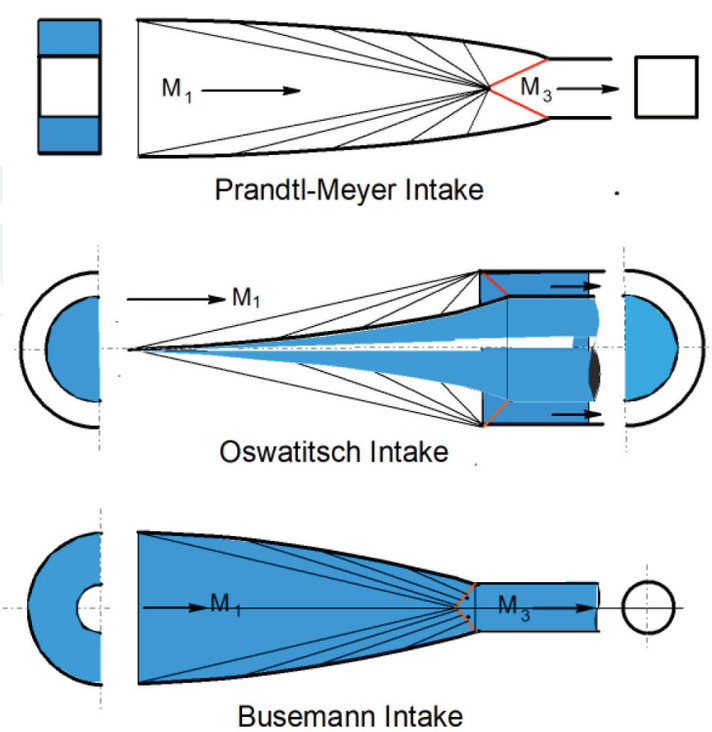

Figure 2.
Schematics of three intakes tested in a gun tunnel at Mach 8.33 [11].

1.4 Streamline tracing: wavecatching, morphing

The design technique of replacing known streamline sheets garnered from simple flows, by solid surfaces to generate aerodynamic shapes, known as "streamline tracing" has been applied to wing-body shapes [20]. The resulting airplane shapes are named "waveriders." The objective in waverider design has been to generate airplane-like shapes that produce high ratios of airplane lift-to-drag force. The same streamline tracing technique, in this case called "wavecatching," is applied to intake flowpath design [4, 7, 13, 14, 21–26] to generate intake surfaces. The objective, in this case, is to generate intake surfaces that capture, support and contain internal flows that have a high performance as supersonic/hypersonic air intakes. Both waverider and wavecatcher applications rest on the fluid-mechanical principle of replacing impervious streamline sheets by solid wall surfaces. In both applications the design starts with the selection of a freestream capture area cross-sectional shape. The shape is projected, as a closed trace, onto the leading shock wave of a prescribed simple flow. In the case of wavecatchers, the trace becomes the leading edge of the intake and the shock wave or Mach wave covers the leading edge of the intake at the design condition. All the mass flow passing through the trace is captured into the intake. The streamtube extending downstream from every point of the closed trace forms the shape of the intake's flowpath. By selecting a suitable shape for the entry flow trace, much design flexibility is available in integrating the resulting engine flowpath with the airframe shape and the intake's exit flow shape to suit the combustor. Pre-selecting the simple flow determines the internal flow as well as the intake performance. The technique is equally applicable to planar and axial flows as well as to non-symmetric flows. The basic wavecatcher technique, when applied to symmetric flows, produces geometrically similar flowpath cross sections. Various methods of morphing can be applied to gradually change the flowpath shape if the entry and exit cross sections are not to be geometrically similar [7, 11, 26]. Two very important extra virtues of the wavecatcher design method are that it produces flow paths with swept leading edges, much like a sugar scoop where, at the design Mach number, the leading shock is everywhere attached to the leading edge; there is no flow spillage. However, at off-design conditions, such a swept leading edge does permit overboard mass spillage during intake flow starting, making otherwise non-startable intakes startable. Experimental results on wavecatcher intake shapes, based on Busemann flow, were presented in [4]. Using streamline tracing methodology, based on the flow in a straight conical duct, the notion of selecting portions of the axisymmetric versions of internal flow was used also in [21–23, 27]. The significant virtues of wavecatcher intakes has been utilized in many subsequent intake studies [10, 13, 21–23, 28–30]. The technique of streamline tracing, to produce modular flowpaths of arbitrary cross sectional shape (wavecatching), results in the following attractive aspects: (a) the total mass flow is divided between individual modules, reducing the mass flow demand of test facilities, both wind tunnels and flight test, (b) thrust vector control is easier to implement with flow in individual modules, (c) highly swept module leading edges make mass flow spillage possible for intake flow starting, (d) module freestream capture shapes are easily integrated with airframe shapes, (e) modules can be raised off the airframe surface so as not to ingest the fore-body boundary layer, (f) properly designed modules are self-startable.

Wavecatching and morphing techniques for modular Busemann intakes will be discussed in Section 7; module startability in Section 8.

1.5 Intake starting/unstarting

For spontaneous ignition and supersonic combustion, the Mach number at combustor entry should be about one-third of the flight Mach number. In a flight Mach number range 4–25, the intake cross-sectional area must decrease by a factor of 5–20. Such a highly convergent duct can support two distinctly different flow configurations at any given supersonic flight Mach number. One flow type produces a bow shock in front of the intake that diverts much flow overboard and, in this case, the intake flow is subsonic with unacceptably low performance. This is termed "subcritical" or "unstarted" flow. The other possible flow configuration has no bow shock, no overboard spillage and is supersonic throughout. This "supercritical," or "started" flow, is required for efficient scramjet engine operation. Attainment of supercritical flow in high contraction ratio intakes present a problem in that the intake flow will not assume the started flow state spontaneously under steady flight conditions. Starting requires that the near-normal bow shock, in front of the unstarted intake, moves downstream into the intake to be "swallowed" and that a stable hypersonic/supersonic flow is established throughout the converging portion of the intake. Spontaneous starting will not occur in intakes whose exit-to-entry area ratio is below 0.6. Unfortunately, startable intakes with exit-to-entry area ratios at or above this value do not produce enough compression to be useful as scramjet intakes. Methods of intake flow starting must be found and implemented for high contraction intake flowpaths. Intake starting is not open to design compromises; it is a critical, non-negotiable requirement that presents challenges and places severe conditions on intake design. Since startability is determined, to a limited extent, by flight Mach number, there is some design flexibility in choosing the start Mach number. Various methods of promoting intake flow starting have been explored in [9, 11, 18, 25, 27, 31–37]. Section 8 presents an analytical approach to the design of spontaneously starting, modular Busemann intakes.

Unstarting of started flow is also a concern in that flight at an extreme angle of attack or at combustor overpressure conditions can cause the intake to regurgitate a stopping shock and the intake flow to revert from a started condition to a condition of unstart. Such an event must be prevented since it is followed by a catastrophic loss of thrust. A review of research progress on detection and control of unstart mechanisms of hypersonic inlets is described in [27, 34].

2. Taylor-Maccoll equation(s) and Busemann flow

Busemann [1] described an axisymmetric, conical flow that starts in the uniform freestream, compresses and contracts isentropically and passes through a conical shockwave to become uniform and parallel to the freestream flow. Courant and Friedrichs [2] make a brief reference to Busemann flow, suggesting its use as an air intake. Molder and Szpiro [3] used the Taylor-Maccoll equations to calculate the inviscid Busemann flow and present a capability/efficiency performance map for the flow as a hypersonic air intake. Experiments, at Mach 8.33, on a full Busemann intake and on modular, wavecatcher surfaces, based on Busemann flow were conducted by Mölder and Romeskie [4] and by Jacobsen et al. [25]. VanWie and Molder [12] suggested applications of the Busemann intake to hypersonic flight vehicles.

The Busemann intake shape is analytically defined by only two numerical parameters [3]. This has made it easily "transportable" and led to its proposed use as a benchmark standard for internal flow CFD verification [38], and a basis for more

general studies of intake flows as well as experiments for such issues as flow starting [18, 25, 27, 31–37], viscous effects [15, 39], truncation [16, 18], drag measurement [11], wavecatcher configurations [13], leading edge blunting [10] and cross section morphing [7]. Viscous effects and truncation and stunting are found in [15, 18, 39]. Experimental results for full and modular Busemann intakes are found in [11, 13, 18, 21, 23, 25, 33, 37, 40]. A four-module Busemann-based intake on a scramjet engine was launched at Mach 5, from a large ballistic gun [41].

The high performance [24] and analytical simplicity of the Busemann intake has made it a subject for some 60 publications.

2.1 Description of Busemann intake flow

The basic Busemann intake surface is axisymmetric (**Figure 3**). It is a converging duct with its axis aligned with the freestream. When started, it captures freestream flow (M_1) in a circular cross section. Since there is no flow deflection at the leading edge there is a zero-strength conical Mach wave (io) from the leading edge at the freestream Mach angle. The flow then starts turning towards the axis, so that flow area decreases and pressure increases in the flow and along the surface (icfs). A maximum turning angle (inflection point) is reached at (f). Turning from (i) to (f) has made the flow convergent so as to compress by convergence. While still convergent and inclined towards the axis, the flow (fs) starts turning away from the axis, passing through a conical shock (os) where it is deflected to become uniform and parallel to the axis at the exit of the intake. This "turning away" of the pre-shock flow lessens the flow deflection requirement of the terminal shock, leading directly to an increase in efficiency. It is this efficiency increase and the convergence in (icfsoi) that contribute directly to the superior performance of the Busemann intake. Flow in the region (icfsoi) is isentropic and irrotational. In the region (icoi) the compression waves from the surface (ic) converge to the focus (o). The compression waves from the rest of the surface (cfs) are incident on the terminal shock. Aside from axial symmetry, this flow is also conically symmetric so that there is a focal point (o) on the axis, from which rays can be drawn, in any direction, such that the flow conditions on any ray are constant. Except for the leading ray (io), the rays are not Mach waves. Axial symmetry makes the rays to be generators of cones so that the flow conditions on circular cones are constant and the conditions are functions of only the conical angle θ (**Figure 3**). All the streamlines are geometrically self-similar, with shapes that are scalable with distance from the origin. Thus, only one streamline, $r = f(\theta)$, needs to be calculated to define the intake surface. Disappearance of the radial dimension (r) as an independent variable, in conically symmetric flow, permits the depiction of all flow conditions on the

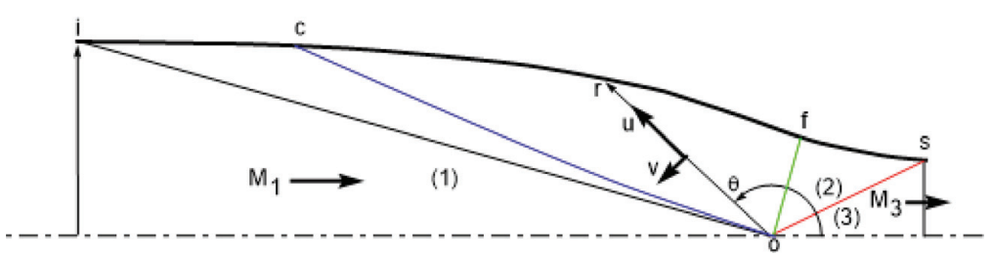

Figure 3.
Busemann intake contour is icfs. io *is a freestream Mach cone.* os *is a conical shock. Uniform entry flow at (1). Uniform exit flow at (3). Supersonic, isentropic, axially and conically symmetric flow from (1) to (2). Flow crosses oblique conical shock from (2) to (3), C-characteristics in* ico *focus at* o. *C-characteristics from* cfs *are incident on the shock along* os. *All streamlines have an inflection point on the cone* fo. *Spherical-polar coordinate system (*r, θ*) is centered at* o *with corresponding radial and angular Mach number components* u *and* v.

single remaining spatial variable—the conical angle, θ. This offers great simplicity in flow analysis where a wide variety of intake surfaces is available for selection of surface shapes that yield both a high compression and a high efficiency for the intake. Furthermore, the presence conical flow means that all shocks, facing conical flow are also conical and therefore of constant strength, at any angular position. The flows are not only uniform but also irrotational—generally a desirable feature for flow that leaves the intake to enter a combustion chamber. These features of conical flow and, in particular, Busemann flow, which is by nature an internal, compressive flow, make the basic Busemann streamline shape an attractive candidate for constructing an air intake for a hypersonic flight vehicle's engine.

2.2 Flow symmetry: coordinate axis: flow direction

Flow which is both axially and conically symmetric is best described in spherical polar coordinates *(r, θ, ϕ)* where *r* is distance measured radially out from the origin, θ is the angle measured counterclockwise from the downstream direction and ϕ is the circumferential coordinate around the axis of symmetry (**Figure 4**). For Busemann flow the origin is at the apex of the conical shock, on the center line of symmetry (xx). The flow velocity components in the radial and angular directions are designated as *U* and *V*. Drawing similar triangles along the streamline, in **Figure 4** gives the streamline equation:

$$dr/d\theta = rU/V = ru/v \tag{1}$$

Busemann flow, and axisymmetric conical flow are governed by the Taylor-Maccoll equation, the same equation that governs the supersonic flow over an axisymmetric cone at zero angle of attack. The original Taylor-Maccoll equation is a non-linear, second order total differential equation with the spherical polar angle, θ, as independent variable and the radial flow velocity, *U*, as dependent variable [42, 43].

$$\frac{\gamma-1}{2}\left[1-U^2-\left(\frac{dU}{d\theta}\right)^2\right]\left[2U+\frac{dU}{d\theta}\cot\theta+\frac{d^2U}{d\theta^2}\right]-\frac{dU}{d\theta}\left[U\frac{dU}{d\theta}+\frac{dU}{d\theta}\left(\frac{d^2U}{d\theta^2}\right)\right]=0 \tag{2}$$

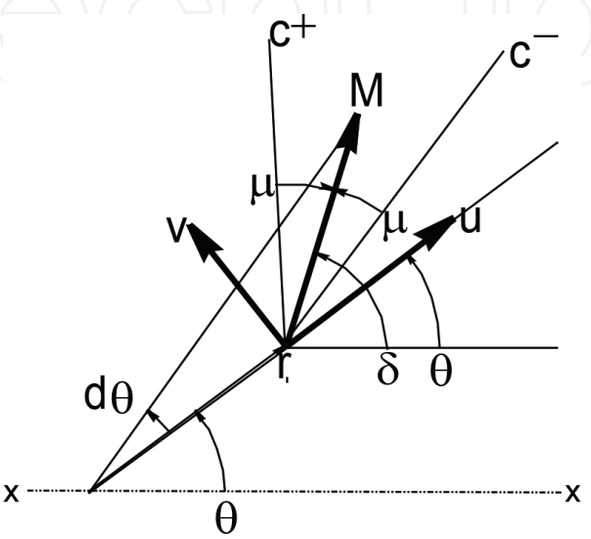

Figure 4.
*The coordinates (*r, θ*); the Mach number (*M*) and its radial and angular components* u *and* v.

This is the model equation that governs steady, axisymmetric, conical flow of a perfect gas. No explicit algebraic solution has been found, nor are there any numerical schemes for solution of the second-order Eq. (2) as given above. However, the equation can be converted to two first order Eqs. (3) and (4), at the price of acquiring the additional dependent variable, V. But the two equations are now amenable to standard numerical solution methods. Most of these solutions have been done with boundary conditions applicable to flow over an axisymmetric cone [42, 43].

2.3 The first-order Taylor-Maccoll equations

The first-order versions of Eq. (1) are the momentum equations, in spherical polar coordinates, in the r and θ directions [44]:

$$dV/d\theta = -U + \frac{a^2(U + V\cot\theta)}{V^2 - a^2} \tag{3}$$

$$dU/d\theta = V \tag{4}$$

where a is the speed of sound that can be written in terms of the velocities and the total conditions through the energy equation. The second of these equations is also the irrotationality condition, implying that conical flows are necessarily irrotational. Explicit reference to the speed of sound and total conditions can be circumvented if the equations are recast so as to have the radial and angular Mach number components (u, v) as dependent variables in place of the corresponding velocity components (U, V). The boundary conditions, when expressed as Mach number components at the up- and down-stream sides of conical shocks, are then applicable directly to the solution of the equations. Also, total conditions, which have no influence on the Mach number solution, do not have to be invoked.

2.4 Mach number components (u, v) as dependent variables

The Taylor-Maccoll (T-M) Eqs. (3) and (4) have been recast in terms of the radial and angular Mach numbers u and v, where $u = U/a$ and $v = V/a$ and a is the local sound speed:

$$\frac{du}{d\theta} = v + \frac{\gamma - 1}{2}uv\frac{u + v\cot\theta}{v^2 - 1} \tag{5}$$

$$\frac{dv}{d\theta} = -u + \left(1 + \frac{\gamma - 1}{2}v^2\right)\frac{u + v\cot\theta}{v^2 - 1} \tag{6}$$

These two equations seem more complicated than their parents (3) and (4). However, it will be shown that the use of Mach number components u and v leads to meaningful and useful physical interpretations from Eqs. (5) and (6). Also, the sound speed has been eliminated as a variable.

In terms of Mach number components, the streamline Eq. (1) is,

$$dr/d\theta = ru/v \tag{7}$$

and the flow Mach number is,

$$M = \sqrt{u^2 + v^2} \tag{8}$$

Having the T-M equations in this form reveals their singular nature at $v = \pm 1$ where the singularity is caused by the $(v^2 - 1)$-term in the denominators above.[1] The term $u + v \cot \theta$, appearing in both numerators, is the component of Mach number normal to the axis. This component is zero for the freestream flow, so that, at the entrance, the Taylor-Maccoll equations take on a 0/0 type singularity and it turns out that $(u + v \cot \theta)/(v^2 - 1)$ has a finite value at the freestream entrance of the Busemann intake.

As a result of using the Mach number variables u and v, the absence of any explicit reference to total conditions, as well as the sound speed, leads to a more straightforward application of the boundary conditions. A standard, fourth-order Runge-Kutta scheme [45] has been used to integrate the Mach number components, u and v form of Eqs. (5) and (6) and $r = f(\theta)$, from Eq. (7). The solutions are identical, to eight decimal places, to similar solutions of (5) and (6) in the velocity variables. Eqs. (5) and (6) govern and describe the flow in a Busemann intake and Eq. (7) gives the streamline/surface shape.

3. Solution of the Taylor-Maccoll equations

Eqs. (5) and (6) are simultaneous, first-order, total differential equations that can be solved by standard methods, such as in Ralston and Wilf [45], for the two Mach numbers u and v in terms of θ. The Mach number M is then found from $M = \sqrt{u^2 + v^2}$ and other thermodynamic values follow from isentropic relations. The shape of the intake surface can also be integrated within the integration routine to give r in terms of θ, $r = f(\theta)$ so that the Cartesian coordinates of the axisymmetric Busemann surface shape are found from $x = r \cos \theta$ and $y = r \sin \theta$.

3.1 Boundary conditions at shock and freestream

Integration of Eqs. (5) and (6) requires the starting values u and v at the value of $\theta = \theta_2$ in front of the shock. A convenient and aerodynamically significant approach is to select the Mach number in front of the shock M_2 and the aerodynamic shock angle θ_{23} as the starting variables. The flow deflection through the shock, δ_{23}, is found from the equation relating Mach number, shock angle and flow deflection [28]:

$$\tan \delta_{23} = \frac{2 \cot \theta_{23} \left(M_2^2 \sin^2 \theta_{23} - 1 \right)}{2 M_2^2 (\gamma + 1 - 2 \sin^2 \theta_{23})} \tag{9}$$

The angular location of the shock, which is the starting value for the variable of integration, θ, is then:

$$\theta_2 = \theta_{23} - \delta_{23} \tag{10}$$

This ensures that the flow behind the shock is parallel to the axis, which is the most common requirement of flow entering a combustor. The starting values for the radial and circumferential Mach numbers are then:

$$u_2 = M_2 \cos \theta_{23} \tag{11}$$

[1] Such singularities are discussed in [29, 45, 46]. Their appearance, in any given flow, should be taken as a warning that whatever symmetry assumption(s) have been made may not hold in the physical airflow.

$$v_2 = -M_2 \sin\theta_{23} \tag{12}$$

The radial variable, r, becomes dependent on u and v and the starting value r_2 at the shock. The value of r_2, the shock's length, is arbitrary at this stage. It determines the scale size of the streamline and its utility becomes relevant when considering morphing and wavecatching in Sections 1.3 and 7. Note that, prior to integration of Eqs. (5) and (6), and calculation of the intake surface shape, we could calculate the intake's efficiency, using the total pressure ratio as measure,

$$p_{t3}/p_{t2} = \left[\frac{(\gamma+1)k^2}{(\gamma-1)k^2+2}\right]^{\frac{\gamma}{\gamma-1}}\left[\frac{\gamma+1}{2\gamma k^2-\gamma+1}\right]^{\frac{1}{\gamma-1}} \tag{13}$$

and the capability from the exit Mach number,

$$M_3^2 = \frac{(\gamma+1)^2 M_2^2 k^2 - 4\left(k^2-1\right)\left(\gamma k^2+1\right)}{\left[2\gamma k^2-(\gamma-1)\right]\left[(\gamma-1)k^2+2\right]} \tag{14}$$

where $k^2 = M_2^2 \sin^2\theta_{23}$ is the square of the shock-normal Mach number component. In fact, we could prescribe a desired efficiency, p_{t3}/p_{t2}, and calculate k^2 from Eq. (13); also prescribe the downstream Mach number M_3 and calculate M_2 by inverting Eq. (14). Then $\theta_{23} = \sin^{-1}(k/M_2)$, $u_2 = M_2 \cos\theta_{23}$ and $v_2 = -M_2 \sin\theta_{23}$. After this, θ_2 and δ_{23} are found as above and the integration performed, on increasing θ, until $(u + v \cot\theta) \geq 0$. The ability to specify the downstream Mach number and an intake efficiency, before doing the integration, makes this approach particularly suitable for preliminary intake design selection. Note, however, that *all is not roses*, since the integration yields a freestream Mach number that may not be the desired one. An iteration, on the input conditions, p_{t3}/p_{t2} and M_3, or k^2 and M_2 has to be performed to arrive at the desired intake design Mach number. This inconvenience is the direct result of, and the price paid for, the convenience and simplicity achieved by imposing the flow to be conically symmetric and by imposing the outflow conditions. It turns out that, using the T-M equations, the flow curvature and gradients of pressure and Mach number can also be found at the shock wave before the complete integration is done (Sections 4.4–4.6).

Eqs. (5) and (6) are then numerically integrated from θ_2 *to* $\theta_1 = \pi - \mu_1$ in an upwind direction with an increasing θ. Since θ_1 is not known *a priori*, the integration is continued until the normal-to-the-axis (cross-stream) Mach number $(u \sin\theta + v \cos\theta)$ becomes zero or positive, indicating that the freestream has been reached. The calculated shape and Mach number contours of such an integration are shown in the top half of **Figure 5**.

Note the conical nature of the contours. The calculated Busemann shape is then used as input to a CFD code to predict the flow as shown in the lower half of

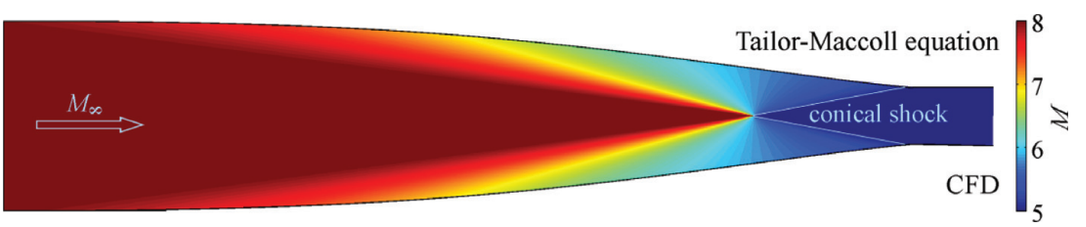

Figure 5.
Flow Mach number contours in the axisymmetric Busemann intake for inviscid flow. Top half is obtained by integrating the Taylor-Maccoll equations. Bottom half is a CFD calculation [by Ogawa] of flow in the same intake shape as the top half.

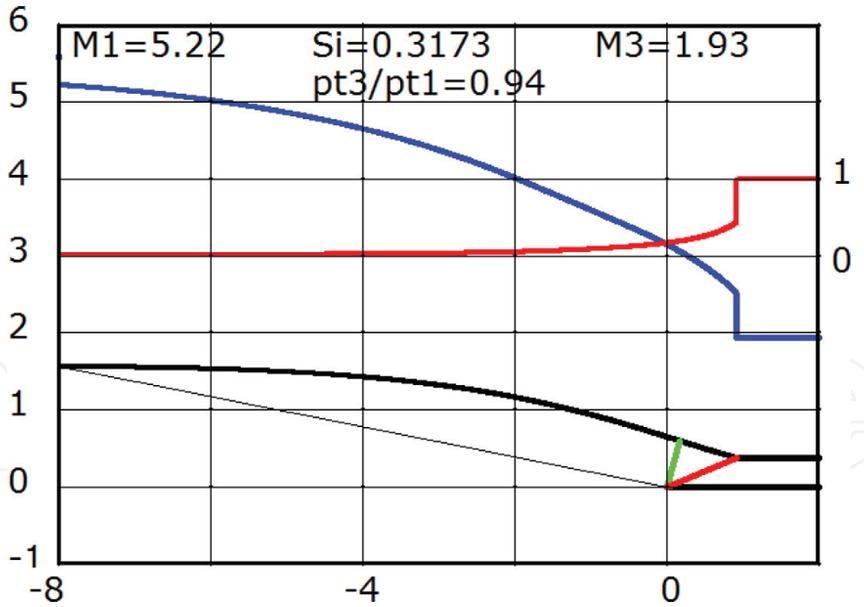

Figure 6.
Busemann intake contour (black curve) with conical shock (red) and cone of inflection points (green). Mach number distribution (blue). Pressure distribution, normalized with respect to exit pressure (red, on the right side ordinate), for an intake that reduces the Mach number from 5.22 to 1.93 with a total pressure recovery of 0.94.

Figure 5. Although the CFD code is not "told" anything about conicality, the conical nature of the flow is well represented by the CFD calculations. Both methods predict a uniform exit flow downstream of the conical shock (courtesy Dr. Ogawa). This is an illustration of the use of Busemann flow as a benchmark for verifying the application of a CFD code to internal flow. Graphical results of an integration of Eqs. 5–7 are shown in **Figure 6** for a Busemann intake that reduces the Mach number from 5.22 to 1.93 with a total pressure recovery of 0.94.

3.2 Singularity at entry

At the entry, Busemann flow joins to the freestream at a conical Mach wave. The Mach number normal to this wave, $v = -1$, which makes both Eqs. (5) and (6) have a zero in their denominators. At the conical Mach wave $u + v\cot\theta$ is also zero so that Eqs. (5) and (6) have a 0/0-type singularity. This makes it impossible to start the integration at a specific freestream Mach number so as to progress in a clockwise (downstream) direction towards the shock. An infinite number of streamlines are possible and unique boundary conditions cannot be specified at the freestream. The starting value of r_2 is arbitrary; it determines the scale size of the streamline and its utility becomes relevant when considering morphing and wavecatching in Sections 7.1 and 7.2.

4. Aerodynamic features of Busemann intake

This section describes some features of Busemann-type intake flow that are unique to axisymmetric conically symmetric flow. First, there is the geometric simplicitly that arises from the axial and conical symmetries. These symmetries require that conditions on a circle, which circumscribes the axis, are constant and conditions are constant also on any circular cone surface whose axis is aligned with the symmetry axis and whose apex is confocal with all other such cones.

Another very important feature is the fact that all solutions of the T-M equations, starting from an acute angled, conical shock, always end up at a straight and parallel freestream flow. Busemann flow would be useless, as the basis for an air intake, if this were not so. This fortuitous feature must be inherent in the T-M Eqs. (5) and (6). This property of the T-M equations holds whether the downstream flow is set to be uniform or not, as long as it is conical.

The downstream end of the Busemann flow has an inflection point where the surface turns away from the axis, towards being parallel with the exit flow. This lessens the flow deflection required from the terminal shock and also lessens the strength and loss produced by the terminal shock. This feature contributes directly to the high efficiency of the Busemann intake flow.

4.1 Free-standing conical shock

In a parallel, uniform, freestream a conical axisymmetric shock is produced by a conical body and the shock strength is proportional to the cone angle. In Busemann flow there is no solid cone, yet a conical shock is produced. This "free-standing" shock is possible because the flow in front of the shock is converging towards the center line and the center line behind the shock is acting as a zero-angle cone to force the flow into a parallel and uniform downstream direction. Such a free-standing conical shock, with uniform post-shock flow, is unique to Busemann flow.

Experiments were conducted, in a Mach 3 wind tunnel, at the Defence Research and Development Canada (Valcartier) laboratories to demonstrate the existence of the free-standing conical shock [40]. Since a full Busemann intake would not start spontaneously in the steady wind tunnel flow and, also, since the shock would be hidden from tunnel optics by a full Busemann duct, only an annular, leading edge portion of the Busemann duct was constructed and tested (**Figure 7b**). The tip of the conical shock, produced by the annulus, is in the region of influence of the annulus and that was sufficient to produce a freestanding conical shock at the center line that was in the field of view of the tunnel optics (**Figure 8**). Compression waves, from the annulus, converge to the center line and reflect as a conical shock as calculated by CFD in **Figure 7a**. No incident shock or Mach reflection is apparent. Calculated post-shock Mach number is 1.48, and pressure is 10.1 and temperature is 1.94 times their freestream values.

The yellow arrow points to the focal point where the converging compression fan and the free-standing conical shock meet. The analytically predicted Busemann flow and its features have been confirmed by both CFD and experiment. The approach presented here is the only method for establishing a centered axial compression followed by a conical shock at the center line in a steady flow. Flow properties inside the apex of the conical shock can be precisely set and the shape of

Figure 7.
(a) Freestanding conical shock at center line, produced by axisymmetric Busemann leading edge annulus in a Mach 3 freestream. CFD calculation by E.V. Timofeev. (b) Busemann leading edge annulus in Mach 3 wind tunnel at DRDC [40].

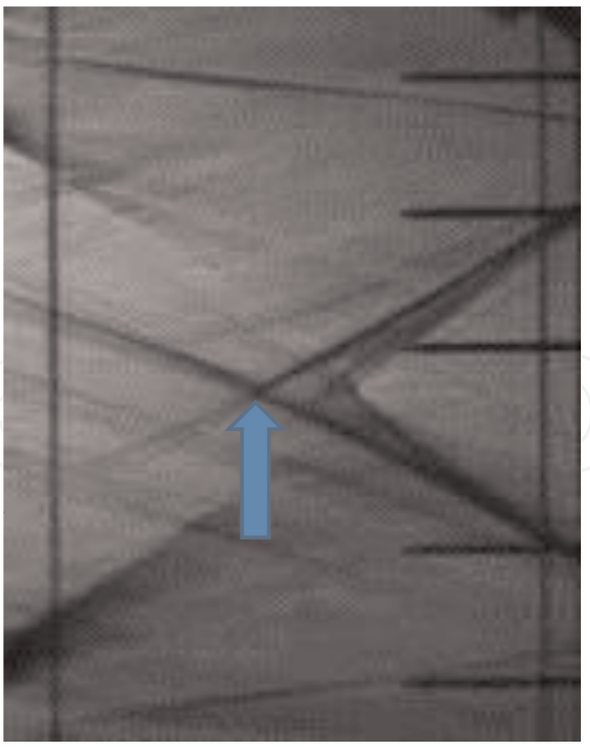

Figure 8.
Freestanding conical shock in Busemann flow at Mach 3 (DRDC). Blue arrow points to apex of conical shock.

the required Busemann annulus calculated so as to create a local high pressure hot spot for igniting a supersonic fuel/air mixture at a precise location.

4.2 Characteristics

Characteristics are two sets of intersecting lines in supersonic flow. The characteristics carry a physical significance in that they delineate the region of space that influences flow conditions at a particular point as well as the region of space that depends on the flow conditions at a point. The characteristic lines are selected such that, along these lines, the governing partial differential equations become total differential, finite difference equations, allowing numerical solutions of the flow-field [42, 46].

Alternatively, once a supersonic flow-field has been calculated by some non-characteristic methods, the characteristic lines can be calculated and superimposed and inferences about influences, causes and effects can be drawn. The α and β or C+ and C− characteristics are inclined at $\pm\mu$ to the local streamlines where $\mu = \sin^{-1}(1/M)$ (**Figure 9**). In polar coordinates the α and β characteristics' shapes are determined by integrating,

$$\left(\frac{dr}{d\theta}\right)_{\alpha,\beta} = r\cot(\delta - \theta \pm \mu) \tag{15}$$

where the plus sign is for the α characteristic and minus is for the β characteristic. For x-y plotting one can integrate the α-characteristics directly:

$$\begin{aligned}(dx/d\theta)_{\alpha} &= r\cos(\delta + \mu)/\cos(\pi/2 - \delta - \mu)\\ (dy/d\theta)_{\alpha} &= r\sin(\delta + \mu)/\cos(\pi/2 - \delta - \mu)\end{aligned} \tag{16}$$

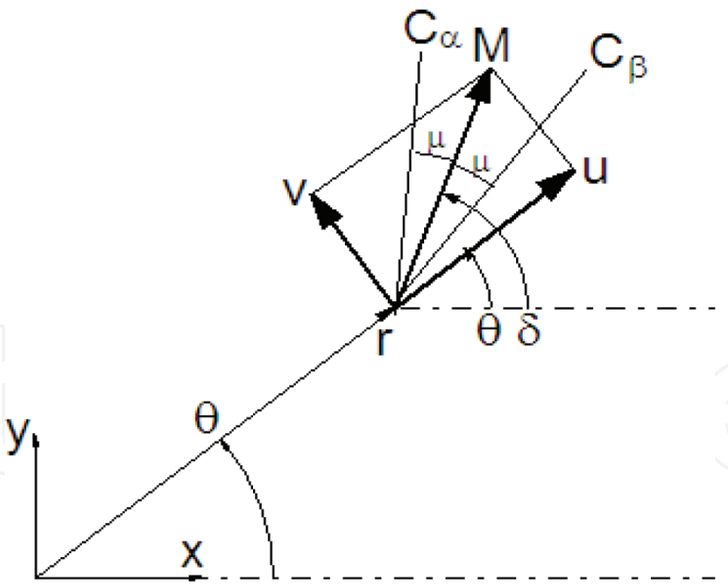

Figure 9.
Characteristics C_α *and* C_β.

and the β-characteristics by:

$$\begin{aligned}(dx/d\theta)_\beta &= r\cos(\delta-\mu)/\cos(\pi/2-\delta+\mu)\\ (dy/d\theta)_\beta &= r\sin(\delta-\mu)/\cos(\pi/2-\delta+\mu)\end{aligned} \tag{17}$$

Integration of the characteristics is easily performed inside the routine for integrating the T-M equations. This method was used to superimpose characteristics on the T-M solution above. Resulting characteristic lines are shown in **Figure 10** for the same Mach 5.22 intake as in **Figure 6**.

4.3 Centered compression fan

The Taylor-Maccoll equations point to the existence of a confocal, conical, compression fan—the axisymmetric analogue to a Prandtl-Meyer fan. Such a fan of coalescing characteristics, preceding a free-standing conical shock, is shown to exist experimentally (**Figure 8**), as well as by CFD calculations (**Figures 7a** and **10**).

The characteristics mesh in **Figure 11** is a schematic overlay on the Busemann flow. The α-characteristics (not shown) all start from the freestream Mach cone and proceed away from the axis to intercept either the surface streamline or the front surface of the shock. The blue and red β-characteristics start at the surface and proceed towards the axis. The first of the β-characteristics is the freestream (1) Mach cone itself, having an inclination μ_1 at the axis. At the shock (2) the remaining characteristics have an inclination $\delta_2 + \mu_2$, different from μ_1. **Figure 11** is a

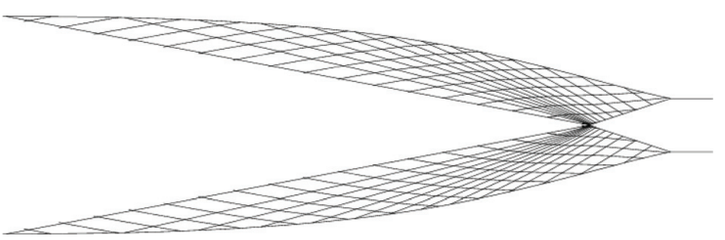

Figure 10.
α *and* β *characteristics network for the Mach 5.22 Busemann intake.* α *characteristics are outbound from the center line and* β *characteristics are inbound. Note convergence of* β *characteristics at center line.*

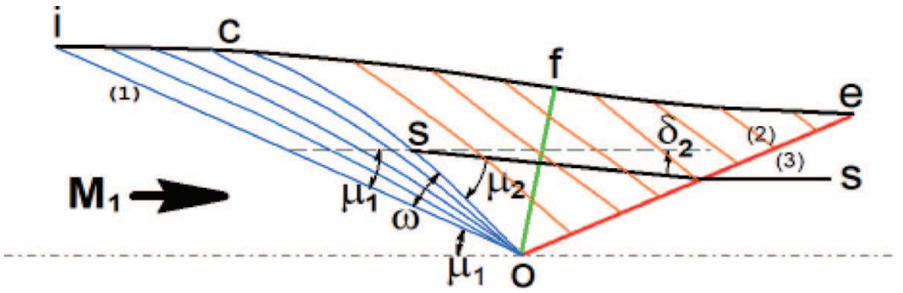

Figure 11.
*Schematic of characteristics in Busemann flow. Centered compression fan (*ioc*). Shock-impinging characteristics (*cfeo*). Subscript (1) refers to freestream conditions, (2) refers to pre-shock conditions. Angles shown are for conditions at* O.

zoomed-in schematic of the conditions at (o) showing a Busemann streamline (icfe) that joins a freestream (1) to the conical shock (oe) at (2). A streamline (ss) passes through the shock. The characteristic (os) and its projection to (c) is the last of the centered β-characteristics (blue) and it is also the first of the β-characteristics (red) that start at the surface and proceed towards the axis but intercepts the shock (oe).

An examination of the inclinations of the characteristics shows that the angular width of the centered compression fan, $\omega = \mu_2 + |\delta_2| - \mu_1$ must be >0, because $\mu_2 > \mu_1$ (since $M_2 < M_1$), so that $\omega > 0$ and the fan must exist. The angular region ω is populated by β characteristics that fan out from (o) to the Busemann streamline along (ic). The fan of β-characteristics contained in (oci) is a centered, axisymmetric compression fan, analogous to the Prandtl-Meyer fan in planar flow. The shape of the last centered characteristic (oc) and the location of (c) can be calculated during the integration of the intake flow when the variable of integration, θ, reaches the value $\pi - (|\mu_2| + |\delta_2|)$. The red β-characteristics from the surface (cfe) all intercept the shock (oe) where a very small, near-apex segment of the shock, is determined by a relatively long length of the Busemann intake surface (ic). The rest of the shock shape is determined by the characteristics from the surface (cfe). This large surface-to-shock length ratio suggests that the leading edge shape is unimportant in determining the overall shock shape. However, a long leading edge surface length contributes to boundary layer growth and viscous losses, providing a reason and an incentive to truncate the leading edge so as to minimize the sum of leading edge shock and boundary layer losses on a practical intake surface. The results presented here give an indication of the extent (ic) to which the conical shock is influenced by a shortening of the intake surface (truncation). A study of viscous/inviscid efficiency loss tradeoffs by truncation or stunting should take direction from the location of point (c). Previous treatment of the centered confocal compression fan or the free-standing conical shock has not been found in the open literature.[2]

4.4 Surface curvature, $D = d\delta/ds$; inflection point

An equation for the curvature of the T-M streamline is derived to show that the streamline can have points of zero curvature—inflection points. The Busemann streamline has two points of zero curvature where one of these points has significance in the starting of a Busemann-type intake. The conical surface containing all inflection points in a typical Busemann flow is shown in green in **Figure 11** where

[2] An analog of this flow exists in planar flow where the region (ioc) is a Prandtl-Meyer compression fan, the region (cof) is then uniform, the shock (ok) is plane and the flow aft of the shock is again uniform. That is the flow topography in the Prandtl-Meyer intake.

the portion of the surface (icf) is turning towards the axis and the portion (fk) is turning away.

To derive an expression for the curvature of the T-M streamline we use the defining equation of the streamline,

$$dr/d\theta = ru/v \tag{18}$$

where u and v are the radial and angular components of Mach number as used in the T-M equations. Taking another θ-derivative of (7) gives,

$$\frac{d^2r}{d\theta^2} = -r\frac{u}{v^2}\frac{dv}{d\theta} + \frac{r}{v}\frac{du}{d\theta} + \frac{ru^2}{v^2} \tag{19}$$

In polar coordinates, (r, θ) the curvature of a planar curve is [28, p. 34],

$$D \equiv \left(\frac{\partial\delta}{\partial s}\right) = \frac{r^2 + 2\left(\frac{dr}{d\theta}\right)^2 - r\frac{d^2r}{d\theta^2}}{\left(r^2 + \left(\frac{dr}{d\theta}\right)^2\right)^{3/2}} \tag{20}$$

Eliminating the derivatives of r with Eqs. (7) and (18) gives,

$$D = \frac{r^2 + 2(ru/v)^2 + r^2\frac{u}{v^2}\frac{dv}{d\theta} - \frac{r^2}{v}\frac{du}{d\theta} - (ru/v)^2}{(r^2 + r^2u^2/v^2)^{3/2}} \tag{21}$$

In this expression the derivatives $dv/d\theta$ and $du/d\theta$ are given by the Taylor-Maccoll Eqs. (5) and (6) so that the streamline curvature is,

$$D \equiv \frac{d\delta}{ds} = \frac{uv(u + v\cot\theta)}{r(v^2 - 1)(v^2 + u^2)^{3/2}} \tag{22}$$

This equation gives the curvature of the T-M streamline in terms of the polar coordinates, r and θ, and the radial and polar Mach number components, u and v. It is plotted as the black curve in **Figure 12**. A number of very interesting and important features, about the T-M streamline, become apparent from an examination of its curvature as given by Eq. (21):

1. D is inversely proportional to r so that when $r \to 0$ then $D \to \infty$. This means that streamlines near the origin of T-M flows are highly curved. This is a necessary condition for flow over a cone, where flow, near the tip and just aft of the conical shock, has to rapidly adjust to the inclination demanded by the cone surface, since the flow deflection produced by the conical shock is insufficient for the flow to be tangent to the cone surface. Similar highly curved streamlines are to be expected near the focal point of Busemann flow. Conical flow is not conically symmetric, i.e., independent of r, when it comes to *gradients* of its dependent variables, such as streamline curvature—the dependence being inversely proportional to r. This inverse dependence on r extends to other flow property gradients as well.

2. There is an asymptotic condition, $(D = 0)$ in the T-M streamlines at $v = 0$. For flow over a cone, $v = 0$ at the cone surface. This confirms that the streamlines become asymptotic to the cone surface as they approach the surface. There is no $v = 0$ asymptotic condition in Busemann flow.

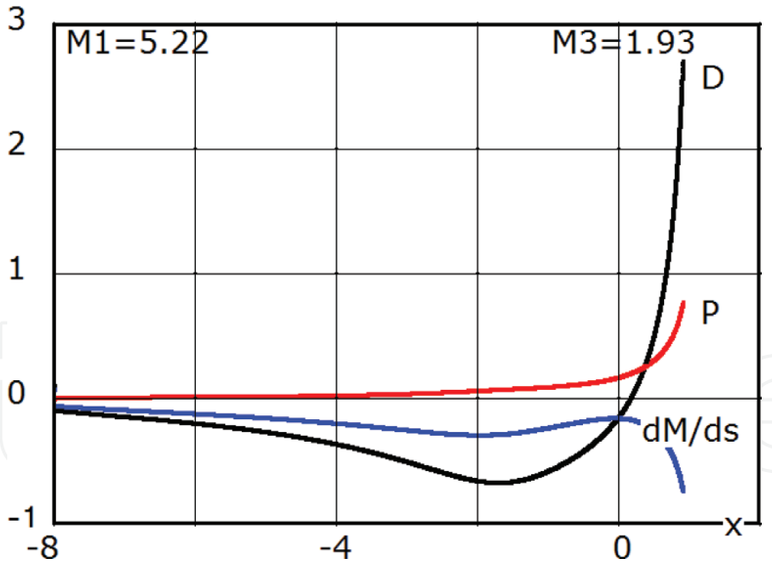

Figure 12.
Surface curvature (D)*, pressure gradient* (P) *and Mach number gradient* (dM/ds)*,* vs. *axial distance (x) in the isentropic part of the Busemann intake. x = 0 is at the apex of the conical shock. Highest values are reached at the corner where x = 0.98.*

3. When $u = 0$ then $D = 0$. This means that the streamline has a point of inflection at the place where the radial Mach number is zero. For flow over a cone the condition $u = 0$ never occurs, so the streamlines are curved monotonically positive. However, for Busemann flow there is a location, $\overline{\theta}$, where the streamline changes from being concave towards the axis (negative curvature) to being convex (positive curvature). The flow changes from turning inward, towards the axis to turning outward, away from the axis. At the inflected surface there is no turning, the flow is purely convergent. Numerical integrations of the T-M equations have shown that $\overline{\theta}$ always lies in the interval θ_2 to $\pi/2$ (first quadrant), somewhat upstream of the Busemann shock, as shown by the green line in **Figure 11**. Every Busemann streamline has an inflection point and, for each intake, these points form a unique conical surface. At this angular location the flow is everywhere normal to the green cone surface, whose half-angle is $\overline{\theta}$, and a conical normal shock can be placed coincident with the green cone since the Mach number is supersonic. This condition leads to an analysis for determining the startability of a wavecatcher Busemann intake according to the following argument: If the bow shock could be coaxed into taking up the inflection position by allowing enough mass spillage to occur between the shock and the inflection location and by restricting the downstream contraction to that allowable by the Kantrowitz criterion for flow starting, then the intake would start. The important variables in the Kantrowitz criterion are the "green" inflection cone surface area, the Mach number in front of the "green" cone and the exit area. These variables are available at the integration of Eqs. (5) and (6) at the streamline inflection angle, $\theta = \overline{\theta}$. If the contraction downstream of the conical normal shock surface does not lead to choking, then the shock moves downstream and the intake starts spontaneously. The starting event and its causes are critical in self-starting supersonic/hypersonic air intakes. It is a conical and axisymmetric example of the starting criterion posed by Kantrovitz for one-dimensional flow, embodying the same principle of flow choking downstream of a normal shock where, in this case, the normal shock is not flat but has a conical shape. Flow just downstream of the conical normal shock at the inflection point is inclined towards the axis. This $(r \rightarrow 0)$-type singularity is similar to the cone-

tip singularity described above; its existence, in the idealized form, has not seen confirmation by experiment or CFD. The cone of streamline inflections is a significant feature for assessing startability of wavecatcher Busemann intakes in Section 8.

4. There is a point of zero curvature also when $(u + v \cot \theta) = 0$. The quantity $(u + v \cot \theta)$ is the component of Mach number normal to the flow axis. For Busemann flow it is zero only where the Busemann flow joins the freestream. Thus, the leading edge of the Busemann flow has not only zero deflection but also zero curvature. Aerodynamically this means that the leading edge wave is neither compressive nor expansive but is a zero-strength Mach wave. The fact that the entering freestream flow is neither deflected nor curved by the Busemann leading edge means that the leading edge of a hypersonic air intake, based on Busemann flow, is ineffective in contributing to the intake's task of reducing the Mach number. This provides an incentive to foreshorten some length of the leading edge surface so as to decrease viscous losses, possibly without incurring serious inviscid flow losses. For M-flow [32] the potential appearance of the condition $(u + v \cot \theta) = 0$ is prevented by the appearance of the $(v \rightarrow \pm 1)$-singularity (described below) so that the post-shock flow never becomes parallel to the freestream. This is unfortunate from a practical viewpoint since it presents no possibility of grafting any of the flows that have a uniform upstream, such as cone or Busemann flows, to the downstream of M-flow. From a fundamental viewpoint it also presents an obstacle to the possibility of conical shock reflection at the center line of symmetry [31].

5. When the angular component of Mach number $v \rightarrow \pm 1$ then $D \rightarrow \infty$; the curvature becomes infinite and the streamline has a cusp or a corner. This indicates a *singularity* or a *limit line* at a corner. Neither cone nor Busemann flow exhibit such a limit line. However, it does occur in both M- and W-flows [32].

6. The quantity $(v^2 + u^2)^{3/2}$, appearing in the denominator of Eq. (21), is just M^3. It is always a positive quantity for all flows and has no drastic characterizing effect on D except to force streamlines to be less curved, to straighten out, at hypersonic speeds. Hypersonic intakes become long and slender.

4.5 Surface Mach number gradient in the flow direction, *dM/ds*

The streamline equation may be written,

$$\frac{ds}{d\theta} = \frac{r}{v}\sqrt{u^2 + v^2} \tag{23}$$

The flow Mach number, M, in terms of its radial and axial components, u, and v, is,

$$M = \sqrt{u^2 + v^2} \tag{24}$$

So that,

$$M\frac{dM}{d\theta} = M\frac{dM}{ds}\frac{ds}{d\theta} = u\frac{du}{d\theta} + v\frac{dv}{d\theta} \tag{25}$$

giving,

$$\frac{dM}{ds} = \frac{v}{r(u^2+v^2)}\left[u\frac{du}{d\theta} + v\frac{dv}{d\theta}\right] \tag{26}$$

where the derivative terms, in the square brackets, are given by the Taylor-Maccoll Eqs. (5) and (6), when multiplied by u and v, respectively.

$$u\frac{du}{d\theta} = uv + \frac{\gamma-1}{2}u^2v\frac{u+v\cot\theta}{v^2-1} \tag{27}$$

$$v\frac{dv}{d\theta} = -uv + v\left(1+\frac{\gamma-1}{2}v^2\right)\frac{u+v\cot\theta}{v^2-1} \tag{28}$$

so that,

$$\frac{dM}{ds} = \frac{v}{r(u^2+v^2)}\left[1+\frac{\gamma-1}{2}\left(u^2+v^2\right)\right]\frac{u+v\cot\theta}{v^2-1} \tag{29}$$

This is the Mach number gradient, expressed in terms of the coordinates (r, θ) and the corresponding Mach number components (u, v), where the Mach number component values come directly from the integration of the Taylor-Maccoll Eqs. (5) and (6). dM/ds is plotted in **Figure 12** (with s measured in the downstream direction).

4.6 Surface pressure gradient in the flow direction, $P = (dp/ds)/(\rho V^2)$

In the isentropic flow, from the freestream to the shock, the gradients of Mach number and pressure are related by [47],

$$\frac{dM}{M} = -\frac{1+\frac{(\gamma-1)}{2}M^2}{\gamma M^2}\frac{dp}{p}$$

$$\text{or} \quad \frac{dM}{ds} = -\left[1+\frac{(\gamma-1)}{2}M^2\right]MP$$

where $\frac{dM}{ds}$ is given by Eq. 26; so that the non-dimensional pressure gradient is,

$$P \equiv \frac{dp/ds}{\rho V^2} = \frac{-v^2}{r(u^2+v^2)^2}\frac{(u+v\cot\theta)}{(v^2-1)} \tag{30}$$

The pressure gradient is expressed in terms of the radial and azimuthal coordinates r and θ and the radial and angular Mach number components u and v. It is plotted in **Figure 12**. This permits the calculation of the surface pressure gradient from quantities obtained in the T-M calculation of Busemann flow.[3] It also means that the surface pressure gradients are known everywhere on the surface of the highly three-dimensional wavecatcher shapes where all the surface gradients are useful as inputs to boundary layer calculations. Towards this end it is noted that, for the flow just upstream of the corner, where the shock impinges, the u and v Mach numbers are given by u_2 and v_2 from Eqs. (11) and (12), so that the gradients immediately before the shock-boundary-layer interaction at the corner can be evaluated just from the prescribed initial conditions using Eqs. (5)–(7), before embarking on a calculation of Eqs. (5) and (6). This enables a selection of initial conditions that is based on considerations involving the shock losses as well as the shock-boundary-layer interaction

[3] These gradient equations are applicable to all types of Taylor-Maccoll flows [48].

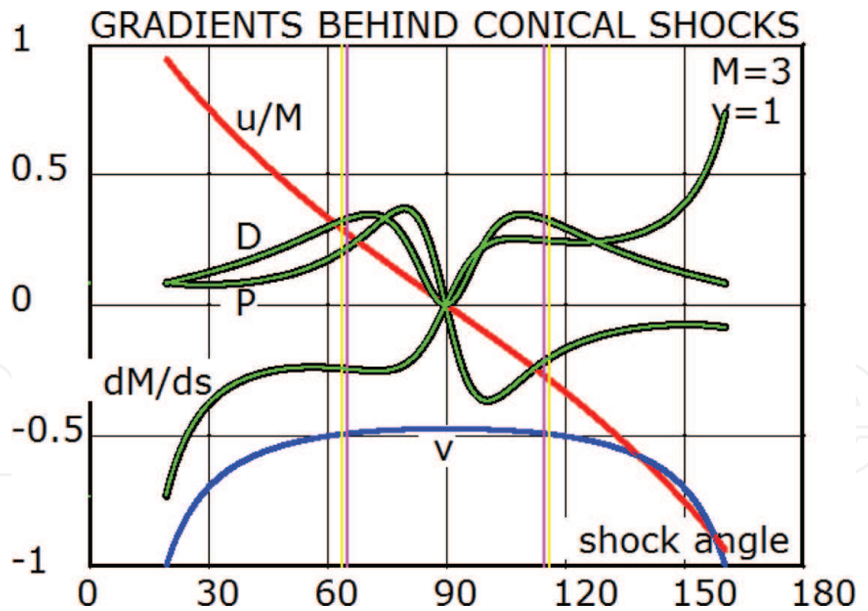

Figure 13.
Mach number components (u, v) *and gradients behind conical shock at Mach 3.*

effects. The analytical expressions for all three gradients have the radial coordinate r in their denominators. This requires the gradients to be the mildest on the intake surface and highest at the origin—a desirable condition for orderly wall boundary layer development on the intake surface.

4.7 Gradients at conical shockwaves

As a check on the various algebraic results we have plotted them against the acute (20–90°) and obtuse (90–160°) angles of conical shocks for Mach 3 in **Figure 13**. The left half of this figure is for acute shocks and the right half is for obtuse shocks, i.e., cone flow and M-flow. u (red) and v (blue) are the Mach number components behind the shock in the (r, θ)-directions. Black curves are for the various gradients from the T-M Eqs. (21), (26) and (27). The green curves are for the same gradients as calculated by Curved Shock Theory (CST) [48]. There is perfect agreement between gradients calculated from the T-M equations and those from CST. This is reassuring since the two methods are based on widely differing theoretical approaches.

5. Performance of Busemann flow as an air intake (inviscid flow)

An integration of the TM-Eqs. (5) and (6) from the initial conditions (10–12) is terminated when $(u + v \cot \theta) = 0$ at the free-stream where we discover the Mach number M_1. The results of many such calculations are shown in **Figure 14** where each complete Busemann intake calculation is represented by a dot. For each case, a value of M_2 is selected, in our case between 1 and 8, and k (the shock-normal component of M_2) is cycled from 1 to M_2. For each M_2 and k the total pressure ratio, Eq. (13), and M_3, Eq. (14), are calculated. Integration of the T-M equations then leads to the freestream at M_1 and a point is plotted on a graph of M_1 vs. M_3 with p_{t3}/p_{t1} as parameter, determining the point's color. Every point in this figure represents a Busemann intake calculation from the downstream shock to the freestream. This graph can be used to select a Busemann intake design based on the desired entry

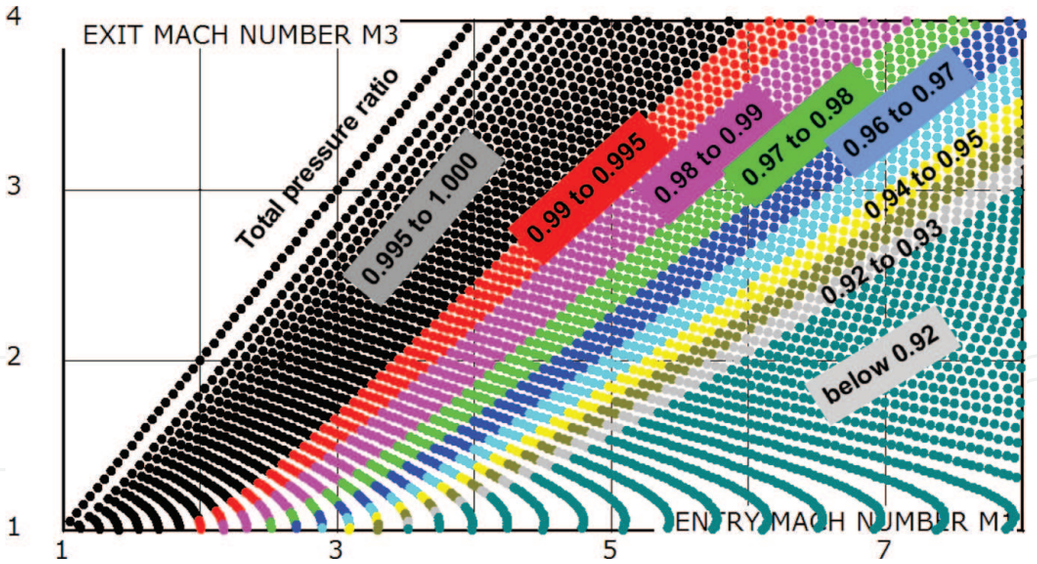

Figure 14.
Inviscid performance of Busemann intake.

and exit Mach numbers and the total pressure recovery. Any two of these parameters determine the third. For example, it is apparent from the graph that a Busemann intake that reduces the freestream Mach number from 7 to 3 does so with a total pressure recovery of 0.95. This graph represents both components of Busemann intake performance, the capability by M_1 and M_3 and the efficiency by p_{t3}/p_{t1}. Tradeoffs between these are workable with this diagram. As an example, a Busemann intake that reduces the Mach number by a factor of three does so with a total pressure recovery of about 0.90. A more refined and elaborate version of such a performance map is found in [3].

6. Boundary layer effects

High performance intakes have to have a very weak leading edge shock. Such a weak shock is inclined at near the Mach angle. This leads to the length-to-height ratio of the intake to be approximately M, the freestream Mach number. So that high performance intakes, including the Busemann intake, tend to become long and slender with large surface areas that have high shear near the leading edge, causing disproportionately high viscous losses. Surface length also leads to thick boundary layers at the exit with losses and the potential for major flow disruptions by boundary layer separation.

A comparison of inviscid and viscous flow in the Busemann intake is shown in **Figure 15** by Mach number contours. The blue, low Mach number boundary layer, appears in the viscous flow. The effect of the boundary layer has led directly to the presence of a shock from the leading edge and a noticeable change in the flow at the center line, a change of exit Mach number from 5.3 to 4.8 and a reduction in total pressure recovery from 0.97 to 0.43. The boundary layer has a significant effect on the inviscid flow even when it appears to stay attached.

Flow displacement by the boundary layer causes a conical shock to appear and focus to a point on the center line ahead of the Busemann flow focal point and a reflected, conical shock appears downstream that impinges on the surface ahead of the corner, **Figure 16**. To restore the inviscid flow topology and pressure distribution of the Busemann flow it is necessary to correct the surface shape of the intake

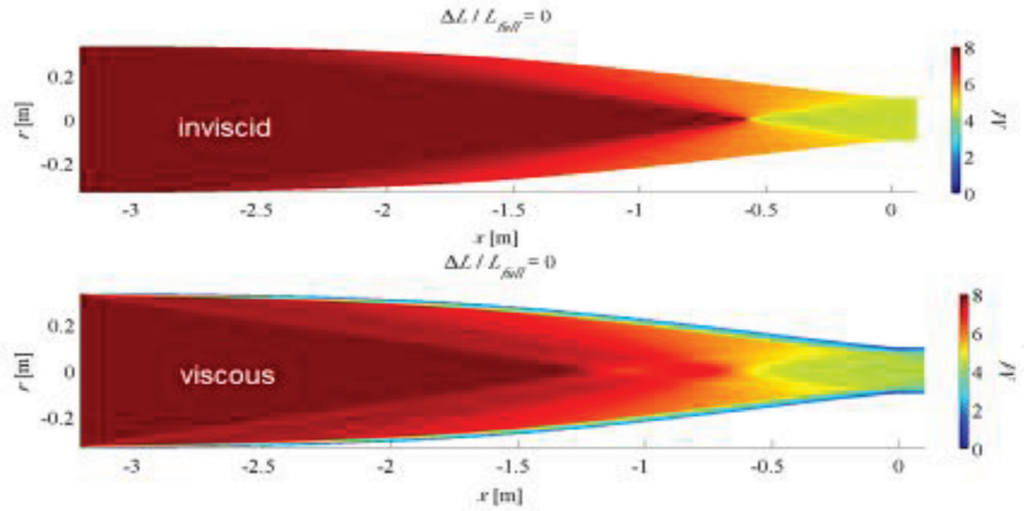

Figure 15.
Inviscid and viscous flow in the Mach 8 Busemann intake at 30 km flight altitude [20].

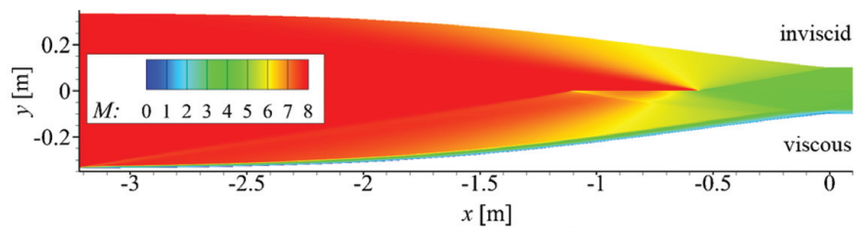

Figure 16.
Mach 8 Busemann intake flows, upper half without and lower half with boundary layer showing the effect of boundary layer on the wave structure of the inviscid flow in the unmodified Busemann intake.

by the boundary layer displacement thickness. The importance of viscous correction methodologies has attracted considerable attention and research efforts as accurate calculation of the boundary layer displacement thickness plays a pivotal role in intake performance assessment. Complex interactions of the shock waves and boundary layers developed on the curved surface of the Busemann intakes pose a challenge to accurate detection of the boundary layer edge. A viscous correction was applied [39, 49] to the full and truncated Busemann intakes by using the displacement thickness obtained through numerical integration of the CFD-generated boundary layer properties. Reasonable detection of the boundary layer edge was attained by examining the total enthalpy profile [50, 51]. Viscous correction is applied typically once only to produce the final geometry. However, the importance of repeating the process, with subsequent iterations, has been highlighted in [52] with the application of an updating procedure of the displacement thickness. The results of correcting for the boundary layer effect are shown in

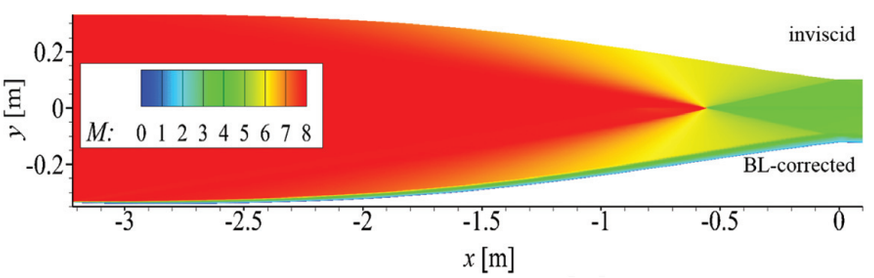

Figure 17.
Upper half contains inviscid Busemann flow. Lower half of flow is contained in a Busemann surface that has been corrected (enlarged) for boundary layer presence [17]. Note successful restoration of BL-corrected flow to be similar to inviscid flow.

Figure 17 where the bottom half of the figure shows the inviscid and viscous flow on a surface that has been obtained by enlarging the inviscid surface by the boundary layer displacement thickness. There is close resemblance between the inviscid and the boundary layer corrected inviscid flows in this figure. Both **Figures 16** and **17** were calculated by H. Ogawa.

7. Geometric modifications to Busemann flow: wavecatching, morphing, truncation, leading-edge blunting

The basic Busemann flow is contained in an axisymmetric streamtube of high contraction. As an intake, such a shape will not start at steady flow conditions. Also the axisymmetric shape may not conform well to the shape of the rest of the airplane surface nor the desired combustor entry and a need arises to modify its cross-sectional shape. Such modifications can be done while still retaining the basic Busemann flow characteristics by tracing the streamlines of the Busemann flow. This process depends on scaling and assembling adjacent, scaled streamlines into streamline sheets that form the wall surfaces of the intake module. The technique produces a wavecatcher intake module. In such constructions a chosen freestream capture cross-section shape becomes mirrored in a smaller, but geometrically similar, intake exit cross-section shape. If done properly, a wavecatcher module has a swept leading edge that captures the leading shock wave and mass flow at design conditions but permits flow spillage and promotes intake flow starting at design and off-design conditions. So a wavecatcher design gets away from an axisymmetric flowpath shape and it also leads to a startable intake as a separate outcome.

The wavecatcher intake shape, that integrates well with the airplane, may have an exit shape that is not necessarily the best shape for the combustor. The combustor shape is very likely wanted to be circular because it is to join to the contiguous combustor duct which is strongest and least aerodynamically lossy when it is circular. There is thus a need to deform the intake flow path gradually from the freestream entry to the exit; typically, from a segment of a circle to that of a full circle or possibly to an ellipse, (**Figure 18**). The method of doing this is called morphing [5, 7, 22, 23].

The Busemann intake has a large amount of surface immediately behind the leading edge. This surface carries a thin boundary layer and a high shear stress, contributing disproportionately to boundary layer losses. The question arises: Can boundary layer losses be decreased by foreshortening some of the surface aft of the leading edge? Realizing that truncation of the leading edge or stunting the intake will result in leading edge flow deflection and shock losses which counter gains achieved from decreased boundary layer losses.

Difficulties of cooling sharp leading edges lead to the adoption of leading edge blunting. Even a small amount of leading edge blunting can have a significant effect on the Busemann flow both in the boundary layer and in the inviscid stream [10].

7.1 Wavecatching (streamline tracing)

The objective of wavecatching is to generate intake flowpath surfaces different from the basic axisymmetric surface of the Busemann flow. The design starts with selecting the desired Busemann flow and calculating its streamline shape, $r = f(\theta)$, as in **Figure 3**. Wavecatcher intake surfaces are then generated from adjacent Busemann streamlines, $r = y(\phi)f(\theta)$ where r is a radial coordinate on the streamline, $y(\phi)$ is a scaling factor that varies smoothly from streamline to streamline and $f(\theta)$ is the shape

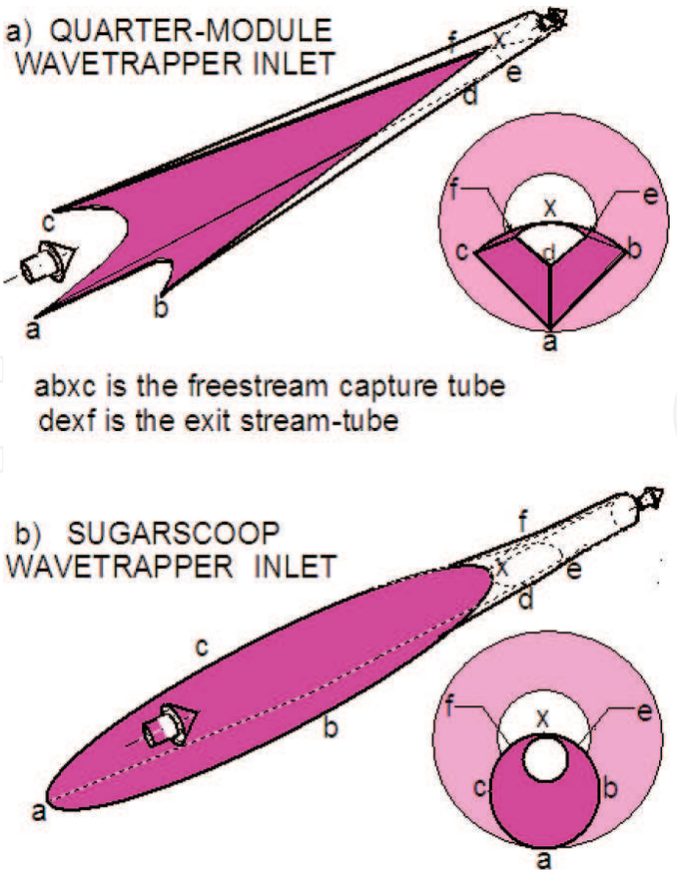

Figure 18.
Wavecatcher intake modules traced from full Busemann flows.

of the Busemann streamline. The scaling factor measures how far the streamline is from the axis of symmetry; its parameter ϕ is unique to each streamline, being the circumferential location of the streamline, the azimuthal angle, measured around the axis. It defines the cross-sectional shape $y(\phi)$ of the freestream capture tube. Note that, on the resulting surface, the variable θ uniquely determines all property values including surface inclination—this being a characteristic of conical symmetry.

Two streamline traced intake modules are shown in **Figure 18**. Both are based on Busemann flow. In **Figure 18a**, the freestream capture tube shape is a quarter circle. The exit is also a quarter circle. Four such modules were placed back-to-back to construct the intake in **Figure 19**. Such four-module intakes were tested in a gun tunnel at Mach 8.33 [4] and this intake, on a scramjet, was launched from a ballistic gun at Mach 5 [41]. **Figure 18b** shows an intake, also traced from Busemann flow,

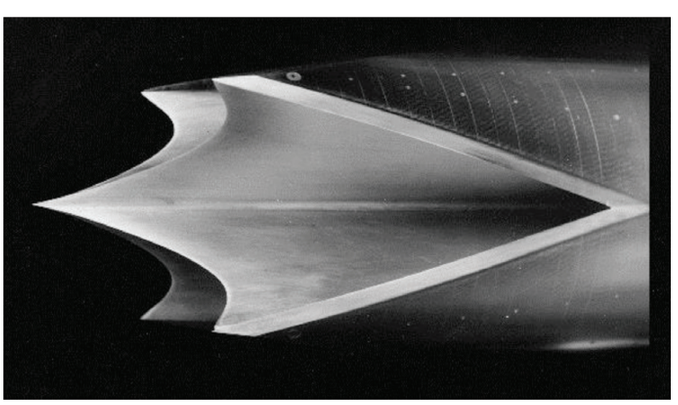

Figure 19.
Four-module Mach 5 scramjet intake based on Busemann flow.

from a circular capture tube shape, where the exit shape is also circular. Such a module was tested in a wind tunnel at Mach 4 [25].

The swept leading edges of modular wavecatcher surfaces permit flow spillage at design and below-design conditions thus promoting intake flow starting. Once started, the apparent three-dimensional intake flowpath contains a started, steady flow with the original Busemann flow properties. These are the two significant virtues of wavecatcher intake modules.

7.2 Morphing (modification of intake flow cross section)

The technique of generating wavecatcher intakes, described in Section 7.1, produces exit flow cross-section shapes that are geometrically similar to the freestream capture streamtube shapes. The purpose of morphing is to produce cross-sectional shapes of the intake flow path that gradually transform the intake's entry shape to a geometrically different exit shape while, as much as possible, preserving the cross-sectional areas as well as the flow characteristics. For example, the flow from a quarter-circle entry is to be morphed to feed a circular combustor.

Figure 20 shows three orthogonal views of a wavecatcher intake and its cross sections when morphed from a quarter-circle to a full-circle. A detailed morphing method, as applied to the Busemann intake streamline $r = f(\theta)$, is pictured in **Figure 21**.

We illustrate by morphing a large, square (blue) inflow cross section into a (red), small circular exit section. A typical morphed Busemann intake design starts from specifying the initial conditions at the Busemann shock. A Busemann streamline $r = f(\theta)$, **Figure 3**, is then calculated from the shock to the freestream, as in Section 3. For each value of ϕ, ranging from 0 to 360°, in a meridional plane, two streamlines are calculated, $r_1 = y_1(\phi)f(\theta)$ and $r_3 = y_3(\phi)f(\theta)$ where $y_1(\phi)$ is the distance from the axis to the freestream capture cross section (blue) and $y_3(\phi)$ is the distance from the axis to the exit flow cross section (red). All the r_1 streamlines project downstream from the leading edge and all the r_3 streamlines project upstream from the trailing edge. The morphed streamline shape, $\bar{r} = \bar{r}(\phi, \theta)$, is then composed of the weighted average of the two streamlines, $\bar{r} = r_1 + g(\theta)[r_3 - r_1]$ where $g(\theta)$ is some assigned morphing function that varies from 0 to 1 as θ varies from the freestream Mach angle to the shock inclination. $\bar{r} = \bar{r}(\phi, \theta)$, then, represents a streamtube surface that joins the square leading edge to the circular trailing

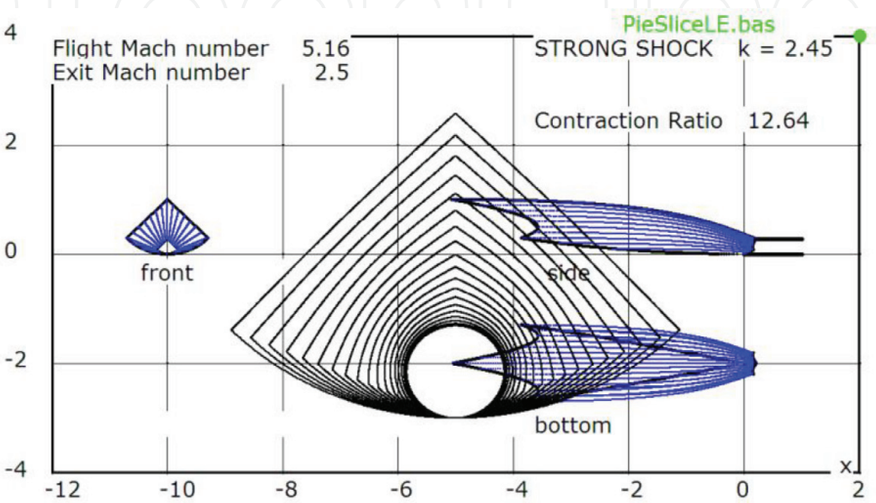

Figure 20.
Three (blue) orthogonal views of a wavecatcher module and cross sections of the modular intake (black) when morphed from a quarter circle to a full circle.

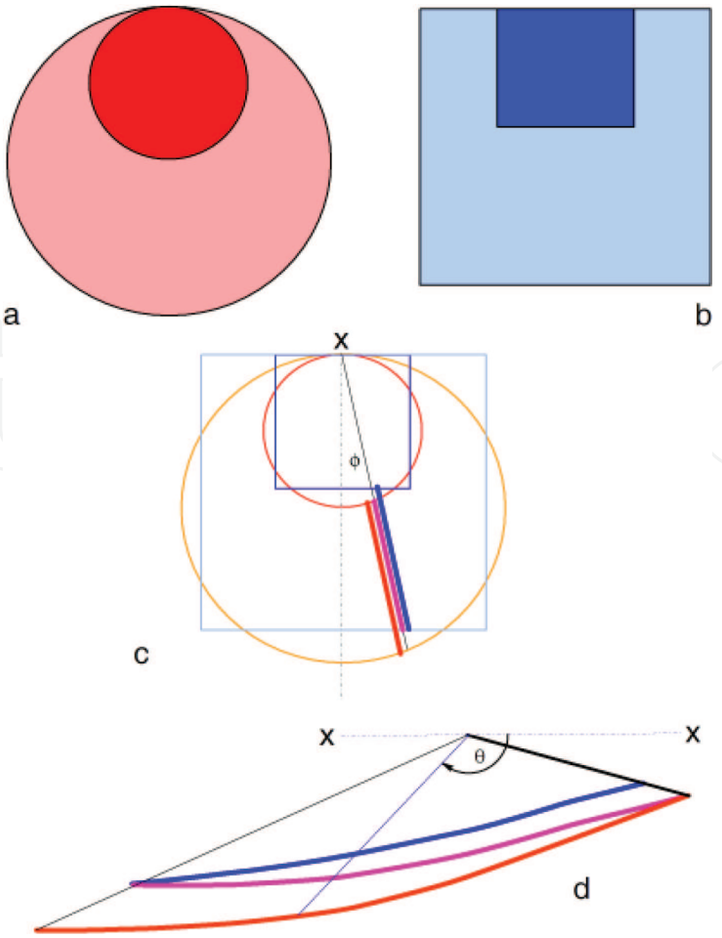

Figure 21.
Morphing of streamline-traced square (blue) and circular (red) streamlines into composite (purple) yielding cross section transition from large blue square to small red circle: (a) is exit geometry; (b) is entry geometry; (c) shows front view of streamlines; and (d) shows side view of streamlines.

edge, as shown in **Figure 21**. The surface grid points are easily calculable from $\bar{r} = \bar{r}(\phi, \theta)$ where $0 \leq \phi < 2\pi$ and $\theta_2 \leq \theta \leq \mu_1$ and the Cartesian coordinates of the surface are:

$$x = \bar{r}\cos\theta \qquad y = \bar{r}\sin\theta\cos\phi \qquad z = \bar{r}\sin\theta\sin\phi$$

Morphing can be used also if the axes of the entry and exit flows are offset, but still parallel.

Although morphing is applied to Busemann flow streamlines, Busemann flow is not preserved in the morphed intake. The morphing process is a purely geometric exercise and its arbitrary nature makes it necessary to verify the morphed intake's flow features and performance, by CFD or experiment. VanWie et al. [7] examined the results of applying various weighting functions and calculated the performance of the morphed intakes using CFD.

7.3 Intake foreshortening: truncation and stunting

As discussed in Section 1, full Busemann intakes are inherently long and hence subject to substantial viscous losses and high structural weight. An examination of the Busemann intake flow-field reveals that the surface at the leading edge has no deflection or curvature in the streamwise direction, presenting no compression of the ingested freestream flow. Thus the leading surface makes little contribution to the task of compressing the flow in the intake. Even worse, it supports a boundary

layer with high shear and attendant losses of intake efficiency. There is then a good reason to expect an improvement in efficiency as a result of eliminating the leading edge surface by foreshortening the intake surface. At the same time one can expect a deterioration of efficiency because the foreshortened intake now has a positive deflection generating a leading edge shock that produces an efficiency loss in the inviscid flow. There is a design trade-off here, between boundary layer and shock losses, which arises from intake foreshortening and it becomes of interest to find an amount of intake foreshortening that minimizes the sum of the boundary layer and the shock losses—maximizes the efficiency. This section describes two representative geometric methods of achieving foreshortening of air intakes, *truncation* and *stunting*. *Truncation* shortens the intake by removing some part of the leading edge surface. The effect of truncation of the Busemann intake was studied in [10, 16, 18]. *Stunting* is longitudinal contraction of the Busemann intake achieved by multiplying all streamwise intake surface coordinates by a constant factor <1. This is linear stunting or telescoping. When applied to a Busemann intake profile, the intake is foreshortened while the flow areas and the zero leading edge flow deflection and curvature are retained. No shock is produced at the leading edge and the overall design contraction is not changed.

CFD-generated intake performance data is presented for a Mach 8, full Busemann intake, flying at an altitude of 30 km, when foreshortened by various amounts of truncation or stunting. **Figure 22** is a plot of intake total pressure recovery against fractional foreshortening of the full Busemann intake calculated by a Navier-Stokes code. The Busemann intake, with applied boundary layer and terminal shock losses lead to a total pressure recovery of 42% for the un-shortened intake.

The effect of truncation on total pressure recovery by various amounts of truncation is shown by the blue curve in **Figure 22**. Truncation produces a modest increase of total pressure recovery from 42 to 46% at near 30% truncation and it appears that intake efficiency is not very sensitive to the amount of truncation.

The effect of stunting, on total pressure recovery, by various amounts is shown by the red curve in **Figure 22**. Total pressure recovery peaks at 47% near 15% foreshortening; decreasing noticeably as stunting increases.

Assessment of truncation and stunting. Both truncation and stunting produce only modest, 4 and 5%, improvements in intake efficiency. However, since the methods are geometrically different, they affect intake capability differently as shown by the compression and contraction ratios in **Figure 23**.

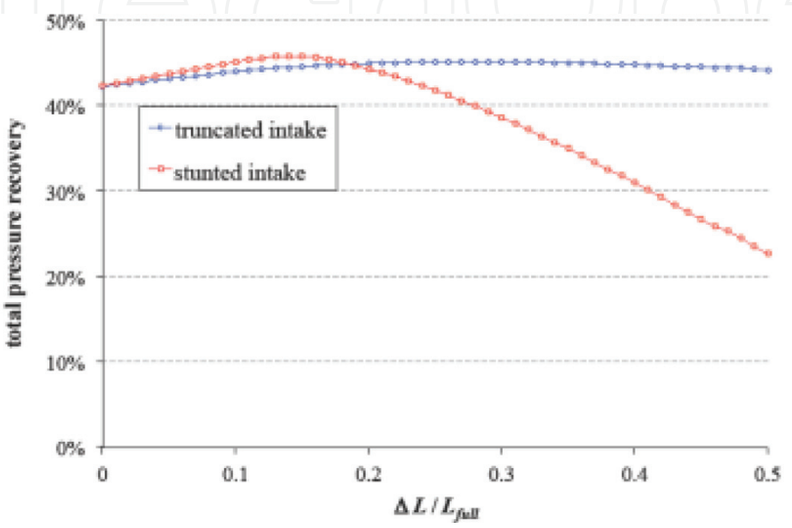

Figure 22.
Effects of truncation and stunting on Busemann intake total pressure recovery.

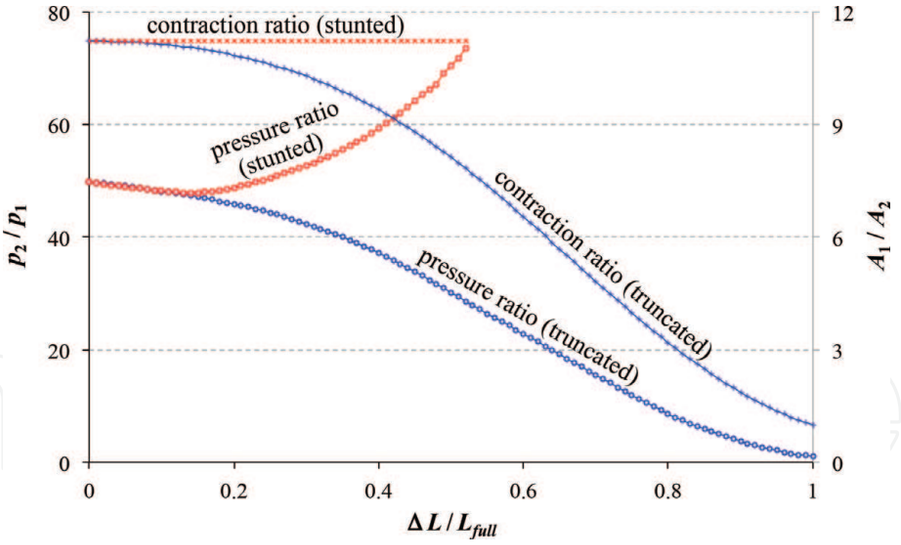

Figure 23.
Variation of intake compression and contraction as caused by truncation and stunting.

Intake performance, both efficiency and capability, are not affected much by considerable amounts of either truncation or stunting. This is due to the fact that the high-loss leading edge boundary layer flow is not eliminated but merely moved downstream. Also there is some increase in inviscid flow losses from the finite angle leading edge from truncation. However, an estimated 15–30% weight saving is available through wall materials elimination resulting from intake fore-shortening. It appears that the significant advantage of truncation and stunting is not to intake performance but to the saving of structural weight. Similar results were found in [10].

7.4 Leading edge blunting

Busemann flow has no deflection at the leading edge so that the leading edge tends to be sharp and thin. Such leading edges are difficult to cool at hypersonic speeds. Transpiration cooling is made possible by a slight rounding of the leading edge. Rounding or blunting affects both the viscous as well as the inviscid flow in the intake [10]. The strong bow shock causes a hot entropy layer to overlay the boundary layer and cause it to thicken. The same shock focuses on the symmetry axis producing a Mach reflection at the center line. It was shown in [10] that a 1 mm diameter leading edge on a 500 mm diameter Busemann intake, flying at Mach 10 and 30 km altitude, is optimal in reducing the viscous and inviscid losses. It seems that the combination of blunting and stunting should be such that the conical shock is kept incident on the Busemann surface corner, so that no reflected shock waves are formed, keeping the exit flow uniform.

8. Startability

The Kantrowitz criterion for intake starting [26] says that the normal shock, in front of an intake duct, will move downstream and out of the duct if the flow at the exit of the duct is not choked—the duct flow will start. This criterion applies to the normal shock at the entry of the duct as well as at any other position in the duct. On a wavecatcher intake, **Figures 18** and **19**, overboard flow spillage will allow the shock to move downstream, over the external/open portion of the intake, until it reaches the V-notch at the beginning of the internal flow. This is made possible by

an effectively large flow area, on the moving, post-shock side, allowing overboard flow spillage. If the Kantrowitz condition, for the shock at the point of inflection, at the V-notch, is satisfied the shock will continue moving downstream, out through the internal flow section, and the intake will start.

The entry area of the internal flow, A_f, is defined as the conical surface at the angular position where the surface is inflected because the flow is normal to the conical surface at the inflection and a stationary, conical, normal shock is compatible with the flow there. The size of this area is available from a Busemann intake calculation. This area is needed for application of the Kantrowitz starting criterion.

8.1 Startability of the weak shock Busemann

Note that, for given M_2 and δ_{23}, Eq. (9), gives two solutions for θ_{23}, for a weak and a strong shock. This leads to the possibility of generating two different Busemann intakes, the weak shock version would have supersonic and the strong shock would have a subsonic exit flow. Because of its supersonic exit flow the weak shock intake is better suited for scramjet application. However, at contractions to be useful for scramjets, the Busemann intake with a weak shock does not start spontaneously or if it does start then it does so for intakes with an insufficient amount of contraction.

The determination of startability for a wavecatcher Busemann intake is as follows. At first we examine the startable weak-shock Busemann flow to show that it does not provide sufficient compression:

a. At a prescribed **weak** shock angle, pre-shock Mach number and exit radius y_3 begin integrating the T-M Eqs. (5) and (6) towards the upstream;

b. Halt the integration when reaching the inflection point, (of) in **Figure 3**, where $u = 0$. Note the Mach number $M_f = v$ and $\overline{\theta} = \theta$ at this point (u is zero here);

c. Calculate surface area of the conical surface at inflection point, A_f;

d. Apply the Kantrowitz criterion to M_f, A_f and A_3 to determine if the internal passage will start.

e. If a start is indicated the intake is practical and integration can be continued to find the freestream (entry) Mach number, M_1, and the other overall performance parameters such as the exit-to-entry area ratio A_3/A_1, the compression ratio p_3/p_1 and the total pressure recovery p_{t3}/p_{t1}.

Many such calculations, starting from *weak shock waves*, (os) in **Figure 3**, were performed with the outcomes plotted on a graph of area ratio, A_3/A_1 *vs.* entry Mach number, M_1, in **Figure 24**. Each result is shown as a dot that is colored green if the totally internal flow Busemann intake duct starts, green or yellow if the wavecatcher Busemann intake module starts (as determined in d) above) and red if there is no start. Curves of the "startability index," $S = (A_1 - A_i)/(A_K - A_i)$, measure the location of a dot on the overall area ratio scale where S = 0 on the isentrope and S = 1 on the Kantrowitz criterion. Intermediate, fractional values, are on curves between these limits. The curve for S = 0.6 seems to well represent the startability limit for wavecatcher Busemann intake designs based on the weak shock condition. As seen from the figure the wavecatcher design lowers the startable area ratio from about 0.6 to 0.4. This is still not good enough. For good engine performance, it is

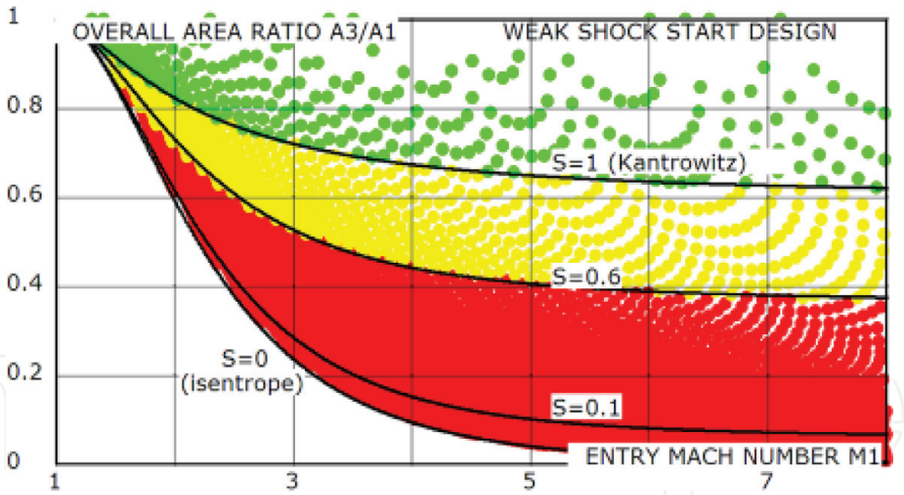

Figure 24.
Busemann intake startability based on weak shock design: green—full Busemann start; green and yellow—wavecatcher start with spillage; and red—no start.

desirable to operate intakes near the curve S = 0.1 in **Figure 24**. Startable weak shock Busemann designs do not produce this amount of contraction—the prospect of obtaining startable full or wavecatcher intakes, with sufficient compression, from weak shock Busemann flows is disappointing.

8.2 Startability of the strong shock Busemann

Startability calculations for the full and wavecatcher Busemann intakes were done also by starting the integration of Eqs. (5) and (6) from strong shock waves, following the (a–e) steps above.

The outcomes are plotted in **Figure 25**. Each result is shown as a dot that is coloured green if the totally internal flow Busemann intake duct starts, green or yellow if the wavecatcher Busemann intake module starts (as determined in d) above) and red if there is no start.

The strong shock version has high overall contraction but low internal contraction so that it will self-start at overall contractions useful to the scramjet as a wavecatcher, but the strong shock and subsonic exit flow are not useful to the scramjet engine. In a wavecatcher module the about-to-start strong shock will be held in place by the appropriate back-pressure. It will move downstream if the

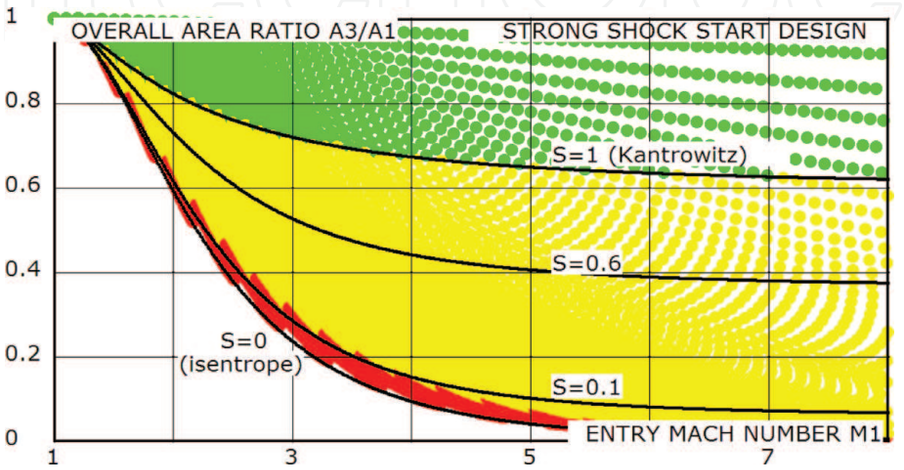

Figure 25.
Busemann intake startability regimes based on strong shock design. green—full Busemann start; green and yellow—module start with spillage; and red—no start.

back-pressure is lowered to be replaced by a weak shock structure. This now opens a possibility. We calculate a Busemann intake module, with a strong shock, such that it starts spontaneously, at a high overall contraction ratio, and then reduce the back-pressure to remove the strong shock and obtain a supersonic exit flow, with a weak shock. This yields an exit flow which is suitable for scramjet operation. In doing this, we note that the flow, from the freestream to the location of the strong shock has not changed as we switch to the weak shock, so that the intake remains on the strong-shock design flow up to the corner while being started. Also, the amount of internal contraction remains the same and we could really start the intake with the weak shock structure in the first place. The strong Busemann shape is really a design tool which leads to a modified Busemann flow but with a started intake of high compression and efficiency having a supersonic exit Mach number-an intake with a high overall contraction but with a low **internal**, startable contraction. The supersonic exit flow is no longer conical although its axial symmetry is preserved.

In comparison to the weak shock case (**Figure 24**) there is a considerable enhancement of startability in the enlarged yellow domain so that starting can be expected near the S = 0.1 curve, which is acceptable for scramjet applications.

The reason for this improvement in startability stems from the fact that, for the strong shock option, the angular distance between the strong shock (at the corner) and the inflection cone is small so that A_f and A_3 areas are close in size, i.e., there is not much internal contraction. This makes it easy for the conical normal shock, at the inflection location, to be swallowed. The strong shock design's aim is to produce a wavecatcher Busemann intake with a high overall contraction ratio and a low internal contraction that starts spontaneously. The calculated shape is compatible with a normal conical shock positioned at the inflection location (angle) and we select the intakes, with internal contractions, that permit the shock to be swallowed. Flow downstream of the inflection shock is subsonic. The strong shock is present only fleetingly during flow starting. After swallowing a weak shock system appears in the exit with supersonic flow downstream. This flow is suitable for a scramjet combustor. Within the calculated strong shock contour the supersonic weak shock flow is no longer conically symmetric and has to be examined via CFD and experiment. The end result is a wavecatcher Busemann intake with a high overall contraction (S $\sim$ 0.1) but with a low internal, self-starting contraction and hence a startable intake and supersonic exit flow.

Figure 26 is a schlieren picture of four quarter-circle Busemann intake modules each with flows started by the unsteady gun tunnel starting flow [4]. Arrow points

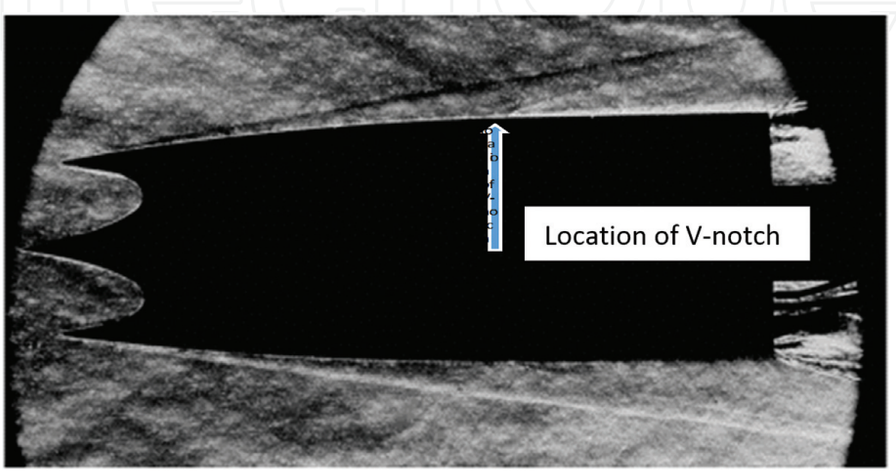

Figure 26.
Impulsively started 4-module Busemann intake in the gun tunnel at Mach 8.33 (model is similar to ***Figure 19****).*

to weak shock emanating from the v-notch in the cowl of one of the modules. Exit Mach number is 5.23.

9. Concluding remarks

A review and summary is presented of hypersonic air intake technology highlighting design objectives, basic flows, airframe integration, flowpath modification and intake flow startability. Taylor-Maccoll equations and Busemann flow are presented as the basis for constructing modular Busemann intakes. The first-order Taylor-Maccoll equations are recast with Mach number components as dependent variables. These equations illustrate the free-standing conical shock, the axisymmetric centered compression fan, characteristics, surface curvature and inflection point, surface pressure gradient, surface Mach number gradient and gradients at conical shock waves. A chart is presented for assessing the performance of the Busemann-flow-based intake on the basis of its capability to reduce Mach number and its efficiency as measured by total pressure recovery. Experimental results indicate that viscous effects cause the total pressure recovery to drop from near 1 to 0.5 for a Busemann intake at Mach 8 and 30 km flight altitude.

Wavecatching (streamline tracing), morphing and foreshortening, as attempts at conditioning and improving the performance of the basic Busemann intake flow, are presented to show that (a) wavecatching is a useful technique to create modular startable intakes; (b) morphing is useful in integrating the intake shape with other geometric requirements of the airframe and combustor; (c) foreshortening leads to minor gains in intake performance but large weight savings; (d) small amounts of leading edge blunting cause large changes in the intake's shock structure.

A novel, *strong shock* method is presented, that uses strong-shock boundary conditions for designing spontaneously startable, modular Busemann intakes of high performance. This analytical approach allows pre-determination of Busemann intake startability; offering great simplicity in the search for flowpath surface shapes that yield startable intakes with high compression, high efficiency and supersonic exit flows. This improved startability is made possible by the wavecatcher's ability to spill mass flow during external compression combined with the moderate contraction of the internal flowpath.

Busemann flow contains unique fluid mechanical features: (a) a flow passage from a uniform, high Mach number flow, to another uniform, lower Mach number flow; (b) internal, convergent flow with an inflected surface; (c) conical flow where high gradients are near the center line and milder gradients are at the walls; (d) an axisymmetric and conically symmetric centered compression fan; (e) a free-standing conical shock, bounding irrotational flow; (f) the last two features combining to preserve conical flow throughout. These are unique and fortuitous virtues, being significant in making the Busemann streamtube and its flow characteristics useful as a basis for designing high performance air intakes for hypersonic airbreathing engines.

Acknowledgements

Most CFD calculations were done by E.V. Timofeev, R.B. Tahir and Hideaki Ogawa. G. Emanuel provided useful comments. Many thanks.

Author details

Sannu Mölder
Ryerson University, Toronto, ON, Canada

*Address all correspondence to: smolder@ryerson.ca

References

[1] Busemann A. Die achsensymmetrische kegelige überschallströmung. Luftfahrtforschung. 1944;**19**(4): 137-144

[2] Courant R, Friedrichs K. Supersonic Flow and Shock Waves. New York: Interscience; 1948

[3] Molder S, Szpiro EJ. Busemann inlet for hypersonic speeds. Journal of Spacecraft and Rockets. 1966;**3**(8): 1303-1304

[4] Molder S, Romeskie JM. Modular hypersonic inlets with conical flow. In: AGARD Conference on Hypersonic Boundary Layers and Flow-fields; Proceedings, No. 30; Cranfield: NATO/ AGARD; 1968

[5] Van Wie DM. Scramjet inlets. In: Scramjet Propulsion. Washington, USA: American Institute of Aeronautics and Astronautics; 2001. pp. 447-511

[6] Grodzovskii GL. Supersonic axisymmetric conical flow bordering on a symmetrical parallel flow through a shock wave. RAE translation of Prikladnaya Matematika i Mekhanika. 1959;**XXIII**(2):379-383

[7] Taylor TM, Van Wie D. Performance analysis of hypersonic shape-changing inlets derived from morphing streamline traced flowpaths. In: 15th AIAA International Space Planes and Hypersonic Systems and Technologies Conference; 28 April 2008–1 May 2008; Dayton, OH: United States; 2008

[8] Duganov VV, Polyakov VV. Hypersonic flow in a converging conical channel. Izvestiya VUZ. Aviatsionnaya Tekhnika. 1976;**19**(2)

[9] Stockbridge RD. Design Requirements for Self-Starting Busemann Diffusers, BBP-78-1 Memo. Applied Physics Laboratory, Johns Hopkins University; 1978

[10] Drayna TW, Nompelis I, Candler GV. Hypersonic inward turning inlets: Design and optimization. In: 44th AIAA Aerospace Sciences Meeting 2006; 9–12 January 2006; Reno, NV: United States; 2006

[11] Molder S, Sullivan PA, McGregor RJ, Sislian JP, Paisley TW. Investigations in the fluid dynamics of scramjet inlets. USAF Contract Report F33615–87-C-2748 and JHU/APL Contract APL602235–0; 1992

[12] Van Wie DM, Molder S. Applications of Busemann inlet designs for flight at hypersonic speeds. In: Aerospace Design Conference; 3–6 February 1992; Irvine, CA, United States; 1992

[13] Matthews AJ, Jones TV. Design and test of a modular waverider hypersonic intake. Journal of Propulsion and Power. 2006;**22**(4):913-920

[14] Sheng YQ. Hypersonic inlet flow computation [MA Sc thesis]. UTIAS, University of Toronto; 1992

[15] O'Brien TF, Colviflet JR. Analytical computation of leading-edge truncation effects on inviscid Busemann-inlet performance. Journal of Propulsion and Power. 2008;**24**(4):655-661

[16] Ogawa H, Shoesmith B, Mölder S, Timofeev E. Viscous correction and shock reflection in stunted busemann intakes, shock wave interactions. Selected articles from the 22nd International Shock Interaction Symposium, University of Glasgow. United Kingdom; 2018

[17] Galkin VM, Zvegintsev VI, Vnuchkov DA. Investigation of annular supersonic inlets with isentropic

compression. Thermophysics and Aeromechanics. 2016;**23**(5):645-655

[18] Ogawa H, Mölder S, Boyce R. Effects of leading-edge truncation and stunting on drag and efficiency of Busemann intakes for axisymmetric scramjet engines. Journal of Fluid Science and Technology. 2013;**8**(2):186-199

[19] Ogawa H, Mölder S. Numerical analysis of hysteresis in mode transition of centerline mach reflection in stunted Busemann intakes for axisymmetric scramjet engines. JAXA Special Publication. 2014;**JAXA-SP-13-011**: 145-150 (in Japanese)

[20] Seddon J, Spence A. The use of known flow fields as an approach to the design of high-speed aircraft. In: Hypersonic Boundary Layers and Flow Fields; AGARD Conference Proceedings No. 30. London, UK: AGARD/NATO; 1968

[21] Keirsey JL, Snow ML. Modular inlet investigation. Quarterly Report AQR/66–1, Aeronautics Division, R&D, APL, Johns Hopkins University; 1966

[22] Smart MK. Calculation of stream-traced hypersonic inlet performance on and off design. In: 21st International Symposium on Shock Waves; Great Kepple Island, Australia; 20-25 July. 1997

[23] Smart MK. Design of three-dimensional hypersonic inlets with rectangular-to-elliptical shape transition. Journal of Propulsion and Power. 1999;**15**(3):408-416

[24] Stockbridge RD. Parametric study of busemann inlets, BBP Memo 77-128, APL, Johns Hopkins University; 1977

[25] Jacobsen LS, Tam C-J, Behdadnia R, Billig FS. Starting and operation of a streamline-traced Busemann inlet at Mach 4. In: AIAA/ASME/SAE/ASEE 42nd Joint Propulsion Conference; 9–12 July 2006; Sacramento, CA, United States; 2006

[26] Kantrowitz A, Donaldson CD. Preliminary Investigation of Supersonic Diffusers. NACA-ACR-L5D20. 1945

[27] Molder S, Timofeev E, Tahir R. Flow starting in high compression hypersonic air inlets by mass spillage. In: 40th AIAA/ASME/SAE/ASEE Joint Propulsion Conference and Exhibit; Fort Lauderdale FL; AIAA 2004-4130. 2004

[28] Ames Research Staff. Equations, Tables and Charts for Compressible Flow. NACA Rep. 1135; 1953

[29] Kreyszig E. Differential Geometry. Mineola, USA: Dover; 1959

[30] Dalitz RH. Some mathematical aspects of compressible flow, Report ACA-20, Australian Council for Aeronautics; 1946

[31] Henderson LF. A critique of the starting phenomena on supersonic intakes. Zeitschrift für Flugwissenschaften.15, Heft. 1967;**15**:2

[32] Najafiyazdi A, Tahir R, Timofeev EV, Molder S. Analytical and numerical study of flow starting in supersonic inlets by mass spillage. In: 43rd AIAA/ASME/SAE/ASEE Joint Propulsion Conference; 8–11 July 2007; Cincinnati, OH, United States; 2007

[33] Timofeev EV, Tahir RB, Molder S. On recent developments related to flow starting in hypersonic air intakes. In: 15th AIAA International Space Planes and Hypersonic Systems and Technologies Conference; Dayton OH; AIAA 2008-2512

[34] Tahir R. Starting and unstarting of supersonic intakes [M.Eng. thesis]. Toronto, Canada: Ryerson University; 2003

[35] Tahir R. Analysis of shock dynamics in supersonic intakes [thesis]. Montreal, Canada: McGill University; 2008

[36] Studzienny A, Molder S, Timofeev E, Voinovich P. Starting of a perforated supersonic inlet: A CFD simulation. In: Proceedings of the 22nd International Symposium on Shock Waves. Imperial College, London UK; 18-23 July. 1999

[37] Tahir RB, Molder S, Timofeev EV. Unsteady starting of high mach number air inlets—A CFD study. In: 39th AIAA/ASME/SAE/ASEE Joint Propulsion Conference and Exhibit; 20–23 July 2003; Huntsville, AL, United States; 2003

[38] Molder S. A benchmark for internal flow CFD code. Computational Fluid Dynamics Journal. 2003;**12**(2):408-414

[39] Walsh P, Tahir R, Molder S. Boundary-layer correction for the Busemann hypersonic air inlet. Canadian Aeronautics and Space Journal. 2003;**49**(1):11-17

[40] Mölder S, Timofeev EV, Lesage EV, Pimentel R. Free standing conical shock. In: Proceedings of 28th International Symposium on Shock Waves, Manchester, England; 2011

[41] Bernhart R. Supersonic martlet/scramjet set for first flight in Canada. Technology World. May 8, 1967

[42] Emanuel G. Analytical Fluid Dynamics, (3rd edition). Boca Raton FL, USA: CRC Press; 2000

[43] Anderson JD. Modern Compressible Flow: With Historical Perspective. New York: McGraw-Hill; 1990

[44] Thompson PA. Compressible Fluid Dynamics. New York: McGraw-Hill; 1971

[45] Ralston A, Wilf HS. Mathematical Methods for Digital Computers. Toronto: John Wiley and Sons; 1960

[46] Zucrow MJ, Hoffman JD. Gas Dynamics. New York: Wiley; 1976

[47] Shapiro AH. The Dynamics and Thermodynamics of Compressible Fluid Flow (Vol 2). New York: Ronald Press; 1954

[48] Mölder S. Curved shock theory. Shock Waves. 2016;**26**(4):337-353

[49] Flock AK, Guelhan A. Viscous effects and truncation effects in axisymmetric Busemann scramjet intakes. AIAA Journal. 2016;**54**(6):1881-1891

[50] Greene F, Hamilton H. Development of a boundary layer properties interpolation tool in support of orbiter return to flight. In: 9th AIAA/ASME Joint Thermophysics and Heat Transfer Conference; 2006

[51] Mcnally WD. BLAYER—Compressible laminar and turbulent boundary layers in arbitrary pressure gradients, Computer Program, LEW-11097. NASA Lewis Research Center; 1994

[52] Carter JE. A new boundary-layer interaction technique for separated flows. NASA-TM-78690. 1978